

Best Available Copy

AD 679978

AEROSPACE REPORT NO.
TR-0200(4220-AQ)-1

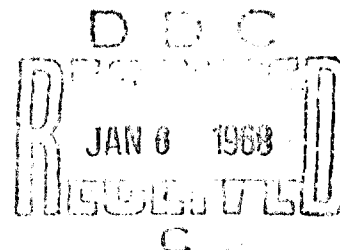
Millimeter-Wave Propagation and Systems Considerations

Prepared by L. A. HOFFMAN
Electronics Research Laboratory

October 1968

Laboratory Operations
AEROSPACE CORPORATION

Prepared for SPACE AND MISSILE SYSTEMS ORGANIZATION
AIR FORCE SYSTEMS COMMAND
LOS ANGELES AIR FORCE STATION
Los Angeles, California



THIS DOCUMENT HAS BEEN APPROVED FOR PUBLIC
RELEASE AND SALE; ITS DISTRIBUTION IS UNLIMITED

Best Available Copy

Air Force Report No.
SAMSO TR-68-445

Aerospace Report No.
TR-0200(4230-46)-1

**MILLIMETER-WAVE PROPAGATION AND
SYSTEMS CONSIDERATIONS**

Prepared by

L. A. Hoffman
Electronics Research Laboratory

October 1968

Laboratory Operations
AEROSPACE CORPORATION

Prepared for

SPACE AND MISSILE SYSTEMS ORGANIZATION
AIR FORCE SYSTEMS COMMAND
LOS ANGELES AIR FORCE STATION
Los Angeles, California

This document has been approved for public
release and sale; its distribution is unlimited

FOREWORD

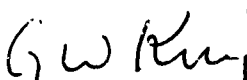
This report is published by The Aerospace Corporation, El Segundo, California, under Air Force Contract No. F04701-68-C-0200 and documents research carried out from March 1963 through June 1968. It was submitted for review and approval on 4 December 1968 to Lt. Jack S. Friedman.

The contributing authors, C. J. Carter, R. A. Miller, Jr., J. M. Stacey, and H. J. Wintroub, are employed at The Aerospace Corporation in the Laboratory Operations Electronics Research Laboratory.

In particular, major contributions to Section III are due to the efforts of J. M. Stacey, C. J. Carter, and R. A. Miller, Jr.; Section V is largely the contribution of H. J. Wintroub.

Experimental work contributing to much of the data content of the paper was performed by D. E. Kind, H. E. King, C. O. Yowell, W. A. Garber, K. H. Hurlbut, and J. D. Michaelson, all of the Electronics Research Laboratory.

Approved



G. W. King, Vice President and
General Manager
Laboratory Operations

Publication of this report does not constitute Air Force approval of the report's findings or conclusions. It is published only for the exchange and stimulation of ideas.

Approved



Jack S. Friedman, Lt., USAF
Project Officer

ABSTRACT

Applications for millimeter waves are discussed, and it is shown how propagation effects enter into systems considerations for the EHF region.

The state of the millimeter-wave art is reviewed as to antennas, sources, amplifiers, and receivers.

Highlighted are two applications, a high-resolution radar, which it is hoped can utilize the inherent advantage of the short millimeter-wavelengths for resolution, and a space-to-space communication system at EHF.

CONTENTS

| | | |
|------|--|----|
| I. | INTRODUCTION | 1 |
| A. | Mapping, Active Radar or Radiometric | 1 |
| B. | Target Sorting | 1 |
| C. | High Tracking Accuracy and Resolution | 5 |
| D. | Reduction of Doppler Navigation Terrain Errors | 5 |
| E. | Reduction of Multipath Errors on Synchronous Links | 5 |
| F. | Spacecraft and Ballistic Missile Terminal Guidance - Altimeter Systems | 5 |
| G. | High Data Rate Communications | 6 |
| H. | High Radar Range Resolution | 6 |
| I. | Reentry Communications | 6 |
| J. | Reentry Observations Through Plasma | 6 |
| K. | Penetration of Blackout Clouds | 7 |
| L. | Freedom from Earth Interference and Jamming | 7 |
| M. | Clutter Elimination at Orbital Altitudes | 7 |
| N. | Secure Satellite-to-Satellite or Aircraft-to- Aircraft Communications at 5 mm | 7 |
| II. | ATMOSPHERIC PROPAGATION EFFECTS | 11 |
| A. | Particulate Scattering and Absorption | 11 |
| B. | Molecular Resonance Absorption | 17 |
| C. | Total Atmospheric Attenuation | 24 |
| D. | Refractive Effects | 24 |
| E. | Significant Observations | 31 |
| III. | STATE OF THE MILLIMETER-WAVE ART | 33 |
| A. | Antennas | 33 |
| B. | Power Sources | 33 |
| 1. | Reflex Klystrons | 37 |
| 2. | Floating Drift Tubes | 37 |
| 3. | Backward Wave Oscillators (BWO) | 39 |

CONTENTS (cont.)

| | |
|--|----|
| 4. Travelling-Wave Tube Amplifiers | 42 |
| 5. Magnetrons | 42 |
| C. Receivers | 44 |
| 1. Detectors | 44 |
| 2. Amplifiers | 46 |
| 3. Mixers | 47 |
| 4. Medium Power Sources | 47 |
| IV. HIGH-RESOLUTION RADAR | 53 |
| A. Approach | 53 |
| B. Experimental Results | 55 |
| C. Critical Considerations and Conclusions | 65 |
| V. SATELLITE-TO-SATELLITE COMMUNICATIONS | 71 |
| A. Early Satellites | 71 |
| B. Satellite Configurations | 73 |
| C. Millimeter-Wave Communication | 76 |
| 1. Satellite-to-Ground Link | 76 |
| 2. Satellite-to-Satellite Link | 79 |
| VI. CONCLUSIONS | 83 |
| APPENDIX A | 85 |
| APPENDIX B | 89 |
| REFERENCES | 93 |

FIGURES

| | | |
|-----|--|----|
| 1. | Spectrum of Aerospace Laboratories Research | 2 |
| 2. | Spectrum Designations | 2 |
| 3. | Zenith Attenuation vs Frequency | 3 |
| 4. | Uses of Millimeter Waves | 4 |
| 5. | Other Uses of Millimeter Waves | 4 |
| 6. | 3.3-mm Radio Heliogram | 9 |
| 7. | Absorption, Scattering, and Total Attenuation Cross Sections of Water Spheres | 12 |
| 8. | Size Distribution as a Function of Rainfall Rate | 14 |
| 9. | Theoretical Attenuation vs Rainfall Rate | 15 |
| 10. | Attenuation in Clouds and Fog | 16 |
| 11. | Attenuation per Kilometer for Horizontal Propagation (From Ref. 5) | 18 |
| 12. | Total Attenuation for One-Way Transmission Through the Atmosphere (From Ref. 5) | 20 |
| 13. | Atmospheric Attenuation Observations | 21 |
| 14. | Day-to-Day Variations in Attenuation | 21 |
| 15. | Uniform Atmosphere Model | 23 |
| 16. | Attenuation of a Stratified Atmosphere | 23 |
| 17. | Visibility Time vs Minimum Antenna Elevation Angle and Maximum Satellite Elevation Angle | 25 |
| 18. | Visibility Time vs Satellite Height and Maximum Elevation Angle | 25 |

FIGURES (continued)

| | | |
|-----|--|----|
| 19. | Atmospheric Index of Refraction Corrections | 26 |
| 20. | Scintillation of Main Beam Power | 28 |
| 21. | Superposed Antenna Patterns, Turbulent Atmosphere | 30 |
| 22. | Slow and Rapid Scan Antenna Patterns, Turbulent Atmosphere | 30 |
| 23. | The 15-ft Antenna | 34 |
| 24. | Characteristics of 15-ft-diam Antenna | 35 |
| 25. | Gain vs Wavelength Summary for Millimeter-Wave Antennas | 36 |
| 26. | Reflex Klystrons CW Power Capability (Production Models - 1970 Estimate) | 38 |
| 27. | Floating Drift Tubes (Two-Cavity Klystrons, Laddertrons) CW Power Capability (Production Models - 1970 Estimate) | 40 |
| 28. | Backward Wave Oscillators and Carcinotrons CW Capability (State of the Art, 1970) | 41 |
| 29. | Traveling-Wave-Tube Amplifiers CW Capability (State of the Art, 1970) | 43 |
| 30. | Magnetrons Peak Power Capability (Pulse Widths < 1 μ sec) (State of the Art, 1970) | 45 |
| 31. | Conversion Loss of Typical Mixers | 48 |
| 32. | Geometry of Various Bulk-Effect Oscillators | 50 |
| 33. | Power Output vs Frequency of Solid-State Sources | 51 |
| 34. | Millimeter-Wave Radar Configuration | 56 |

FIGURES (concluded)

| | | |
|--------|---|----|
| 35. | Short-Range Millimeter-Wave Radar Test Setup | 59 |
| 36. | Comparison of Open-Loop (Top) and Closed-Loop (Bottom) Beat-Frequency Deviations; FM Feedback Loop. Low-1, $T = 1$ msec, $\tau = 0.8$ μ sec | 59 |
| 37. | Phase-Lock Sweep Linearization | 61 |
| 38. | Comparison of Open-Loop and Closed-Loop Beat-Frequency Deviations; Phase-Locked Loop. Low-1, $T = 1$ msec, $\tau = 0.8$ μ sec | 61 |
| 39(a). | Beat-Frequency Spectrum Open Loop | 62 |
| 39(b). | Beat-Frequency Spectrum Phase-Locked Loop | 62 |
| 40. | Radar Equipment (Short-Range Test Setup). | 64 |
| 41. | Mixer Unit | 67 |
| 42. | Electromechanical TR Switch | 68 |
| 43. | Beam-Waveguide System | 69 |
| 44. | Mutual Visibility for Low-Altitude and Synchronous-Altitude Satellites | 72 |
| 45. | Ground Terminal Separation vs Satellite Altitude for Mutual Visibility | 74 |
| 46. | Global Coverage Relay System | 75 |
| 47. | Communication Link Performance Summary Satellite-to-Ground Terminal | 78 |
| 48. | Communication Link Performance Summary Satellite-to-Satellite Relay (70 GHz). | 81 |

I. INTRODUCTION

For the purpose of this report, the millimeter-wave region is defined to be between the limits of 10 and 1 mm, or from 30 to 300 GHz. This region is also known as the Extremely High Frequency (EHF) region (Figures 1 and 2). The major portion of the research in the Aerospace Corporation Electronics Research Laboratories has been done in the 94-GHz (3.2 mm) atmospheric window (Figure 3) at a frequency approximately 10 times X-band frequencies. Important new information has been obtained by experimental system measurements in the 60-GHz (5 mm) oxygen absorption complex, and a radiometric capability has recently been added at 220-GHz (1.36 mm), located at the center of another atmospheric window.

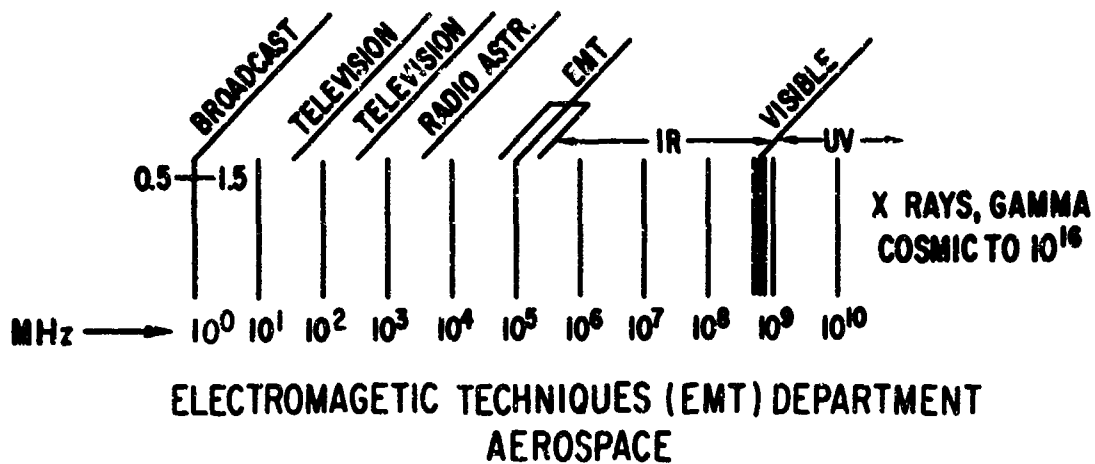
Potential applications for millimeter waves (Figures 4 and 5) are briefly described in this section. Although not an exhaustive list, most of the applications that are proposed by those working in this region as a partial justification for their research are included.

A. MAPPING, ACTIVE RADAR OR RADIOMETRIC

Narrow beamwidths and high gain achievable with reasonable size antennas make high-resolution mapping attractive at millimeter waves. Passive detection of missiles by radiometric means is possible since an intermediate product of all rockets is the free radical, an unstable but electrically neutral particle, which emits electromagnetic energy in the millimeter region of the spectrum.

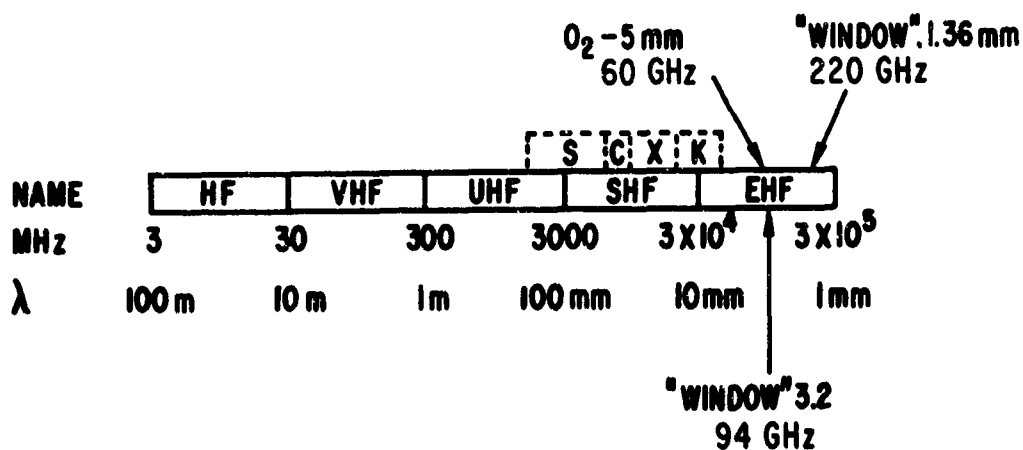
B. TARGET SORTING

In a multiple target environment, target sorting is easier with narrow



60 GHz (5 mm)
94 GHz (3.2 mm)
220 GHz (1.36 mm)

Fig. 1. Spectrum of Aerospace Laboratories Research



5-mm WAVELENGTH \approx 0.2 in.
3.2-mm WAVELENGTH \approx 1/8 in.
1.36-mm WAVELENGTH \approx 0.05 in.

Fig. 2. Spectrum Designations

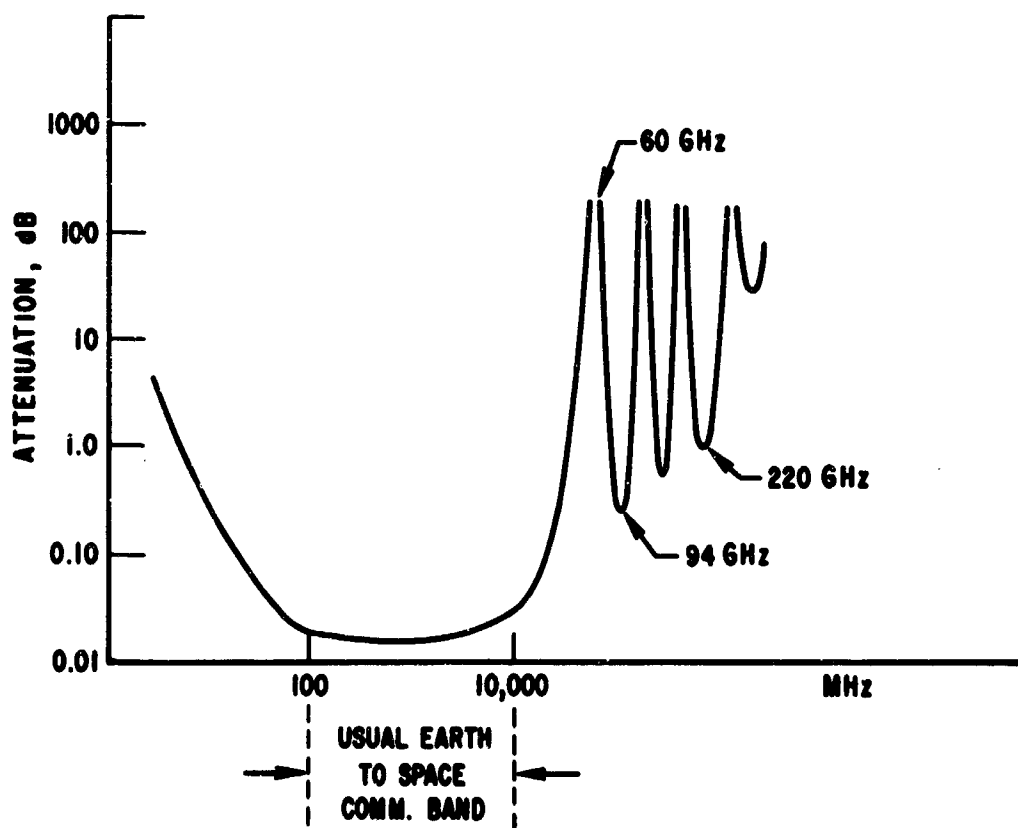


Fig. 3. Zenith Attenuation vs Frequency

NARROW BEAMWIDTH, HIGH DOPPLER SENSITIVITY, LOW SIDELOBES

Mapping—Active Radar or Radiometric
Target Sorting
High Tracking Accuracy/Resolution
Reduction of Doppler Navigation Terrain Errors
Reduction of Multipath Errors on Synch Links
Spacecraft Terminal Guidance—Altimeter Systems

HIGH GAIN ANTENNAS, LARGE BANDWIDTH CAPABILITY

High Data Rate Communications
High Radar Range Resolution

Fig. 4. Uses of Millimeter Waves

PROPAGATION THROUGH HIGH ION DENSITIES

Reentry Communications
Reentry Observations Through Plasma
Penetration of Blackout Clouds

O₂ ABSORPTION AT 5 mm, NEW SPECTRUM USAGE

Freedom From Earth Interference and Jamming
Clutter Elimination at Orbital Altitudes
Secure Sat-Sat or Air-Air Communications

Fig. 5. Other Uses of Millimeter Waves

beamwidths that illuminate a smaller field of view, thus reducing clutter and masking. Target sorting is also easier with a high Doppler sensitivity, by velocity discrimination of even small velocity differentials. The two way Doppler $f_d = 2v/\lambda \approx 200 \text{ Hz/ft/s}$ at 94 GHz.

C. HIGH TRACKING ACCURACY AND RESOLUTION

Again, narrow beamwidths and high Doppler sensitivity achievable at millimeter waves with small antenna having high gain make this application attractive. The Doppler measurement precision σ_v is directly proportional to wavelength, other things being equal; i.e., $\sigma_v = \lambda/4 T\sqrt{S/N}$ where T is the pulse length in seconds.

D. REDUCTION OF DOPPLER NAVIGATION TERRAIN ERRORS

Spectrum spreading of the returned signal is minimized because less area is illuminated by the beam for a given antenna size. Also, the dependence of the reflection coefficient on the angle of incidence is reduced since the ground looks less smooth at the higher frequencies.

E. REDUCTION OF MULTIPATH ERRORS ON SYNCHRONOUS LINKS

Narrow beamwidths and low sidelobes make possible long distance transmissions without multipath signal reception, which causes phase errors and fading in synchronizing links of widely space interferometer systems. These systems are used for guidance and trajectory measurements.

F. SPACECRAFT AND BALLISTIC MISSILE TERMINAL GUIDANCE - ALTIMETER SYSTEMS

The advantages previously mentioned apply here along with the possibility for small, lightweight, compact equipment as required for spacecraft hardware once solid-state power sources become available.

G. HIGH DATA RATE COMMUNICATIONS

The theoretical data rate achievable for a given S/N is directly proportional to the available bandwidth β ; i.e., the data rate is equal to $\beta \log_2(1 + S/N)$. A 10% bandwidth at 94 GHz is equivalent to the entire spectrum now being used up to X-band.

H. HIGH RADAR RANGE RESOLUTION

Range resolution and accuracy are dependent on the spectrum width, other things being equal; i.e.,

$$\text{range error precision} = \sigma_r = c/(2B\sqrt{S/N})$$

Laser ranging devices are limited by atmospheric propagation effects that produce refraction, scintillation, and attenuation, while conventional radar in the present microwave bands lacks the theoretically high resolution of shorter wavelengths wherein scatterers on the order of the wavelength in extent return distinct echoes. Radar in the millimeter band would be a good compromise.

I. REENTRY COMMUNICATIONS

Reliable communications with manned reentry vehicles during the reentry phase is highly desirable. A fundamental requirement for the propagation of electromagnetic radiation through a plasma is that the signal frequency be above the plasma resonance frequency.

J. REENTRY OBSERVATIONS THROUGH PLASMA

If the plasma can be penetrated, then perhaps some indication of size and shape can be determined for identification purposes.

K. PENETRATION OF BLACKOUT CLOUDS

An enemy precursor nuclear explosion could be used to black out radar detection of approaching enemy vehicles. Millimeter-waves may be able to penetrate these blackout clouds so that these targets could be detected.

L. FREEDOM FROM EARTH INTERFERENCE AND JAMMING

Absorption is so high, at certain regions of the 5-mm absorption complex, that penetration of the atmosphere so as to interfere with high-flying aircraft or satellites is virtually impossible.

M. CLUTTER ELIMINATION AT ORBITAL ALTITUDES

A satellite surveillance system at 5 mm for detecting vehicles emerging from the atmosphere would not suffer from clutter and noise due to ground reflections since the energy would be completely absorbed. Other absorption bands exist at higher frequencies of equal potential use.

N. SECURE SATELLITE-TO-SATELLITE OR AIRCRAFT-TO-AIRCRAFT COMMUNICATIONS AT 5 mm

Since no radiated energy would reach the earth, communication would be private from one vehicle to another. Privacy could be further enhanced by the use of highly directional antennas of a relatively small size.

Other potential applications include localized communication systems where communications between points at short ranges could be kept private by operating in the absorption bands where high absorption would prevent penetration beyond the desired range. Such systems are not only private but are also jam resistant.

Another field just beginning to reap benefits from millimeter-wave receiver advances is radio astronomy. Work of this type has been done at

frequencies lower than 30 GHz. The large ground antennas now available, and useful at millimeter waves, have made important contributions. The high resolution permits the preparation of radiometric maps of the moon and sun. The map in Figure 6 was taken at 94-GHz (3.2 mm) and offers a unique high-resolution display of the deep chromosphere where millimeter emission occurs and where solar flares originate. As such, these maps may be a key to solar flare prediction. Increases in temperature observed at 3.2 mm have been observed prior to flare activity and may be correlated with particle emission that is dangerous to man in space. As millimeter-wave equipment continues to evolve and improve, and as space laboratories become available above the absorbing atmosphere, many atomic and molecular transitions manifesting themselves in the millimeter-wave regions will be useful for radio astronomical observations and investigations.

In spite of this long list of useful applications with which to relieve an already overcrowded spectrum, there are, at present, no established millimeter-wave communications systems for space. A few experimental systems have been developed, and forerunner studies have been funded for satellite-to-satellite communications systems investigations. The lack of adequate sources and detectors has been a deterrent to research and development in this part of the spectrum.

Current advances in technology are removing these obstacles, thereby justifying a careful evaluation of millimeter waves for communications and other systems. In the following sections, recent advances toward implementation of two previously mentioned systems will be highlighted: a

high-resolution Space Object Identification (SOI) radar at 94 GHz and a
satellite-to-satellite communication system.

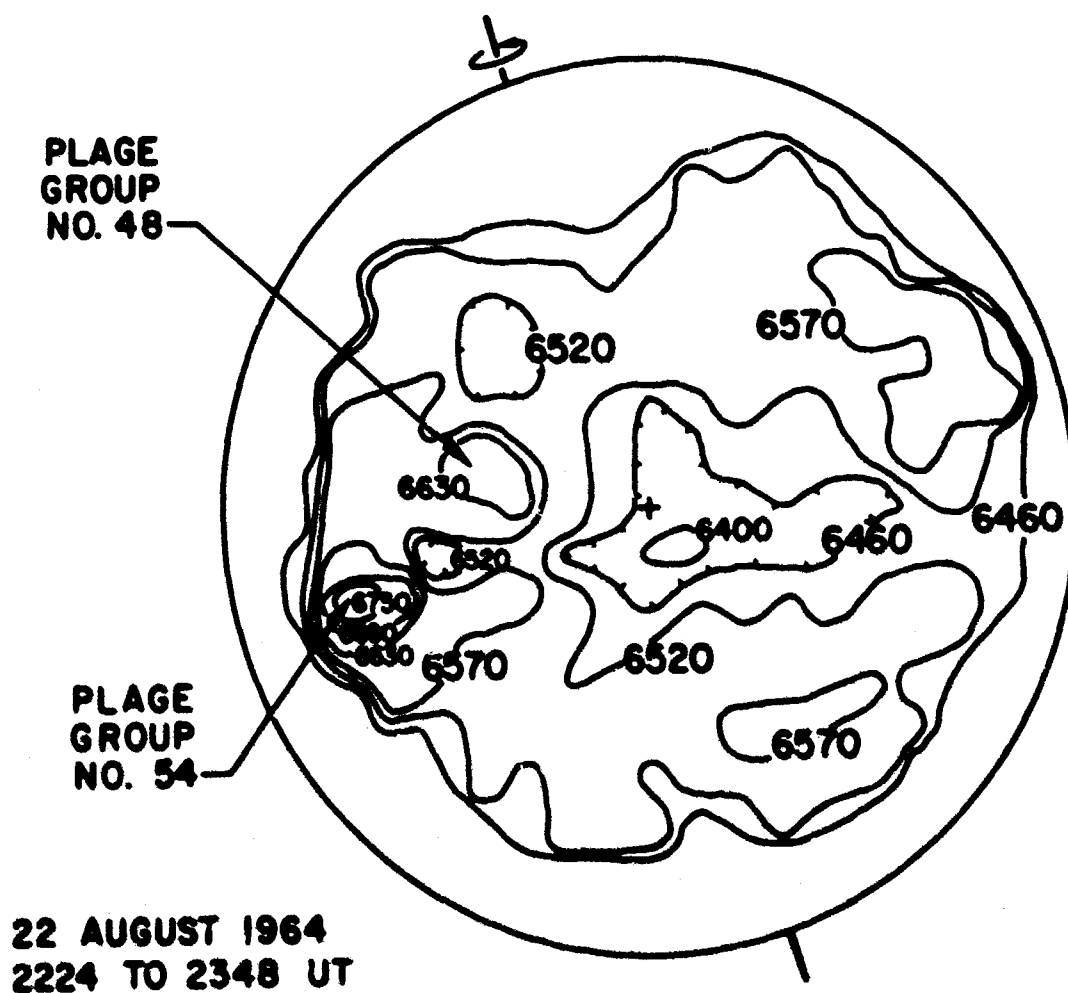


Fig. 6. 3.3-mm Radio Heliogram

II. ATMOSPHERIC PROPAGATION EFFECTS

The earth's atmosphere strongly affects the propagation of millimeter waves. Three types of phenomena are observed: (1) particulate scattering and absorption, (2) molecular resonance absorption by oxygen and water vapor, and (3) scattering and refraction due to spatial inhomogeneities in the atmospheric index of refraction. The order of listing corresponds to the potential severity of the effect, as will be demonstrated in the following paragraphs.

A. PARTICULATE SCATTERING AND ABSORPTION

The atmospheric particles that appreciably scatter or absorb millimeter-wavelength electromagnetic waves are condensed water droplets in rain, clouds, or fog, ice particles in snow or hail, and aerosols. The attenuation due to these particles can be estimated using theoretical calculations of scattering and absorption coefficients for spheres (Mie scattering theory) and appropriate assumptions concerning particle size distributions [1]. The attenuation expressed in dB per unit length is

$$\alpha = 4.34 \int N(D) Q_t(D) dD$$

where $Q_t(D)$ is the sum of the absorption and scattering cross sections for a particle of diameter D , and $N(D) dD$ is the number of particles having a diameter between D and $D + dD$ per unit volume. The cross sections are computed using the Mie series coefficients. Figure 7 shows absorption, scattering, and total attenuation cross sections [2] for water spheres at 3-mm and 10-mm wavelengths. These plots show the critical nature of D/λ . For

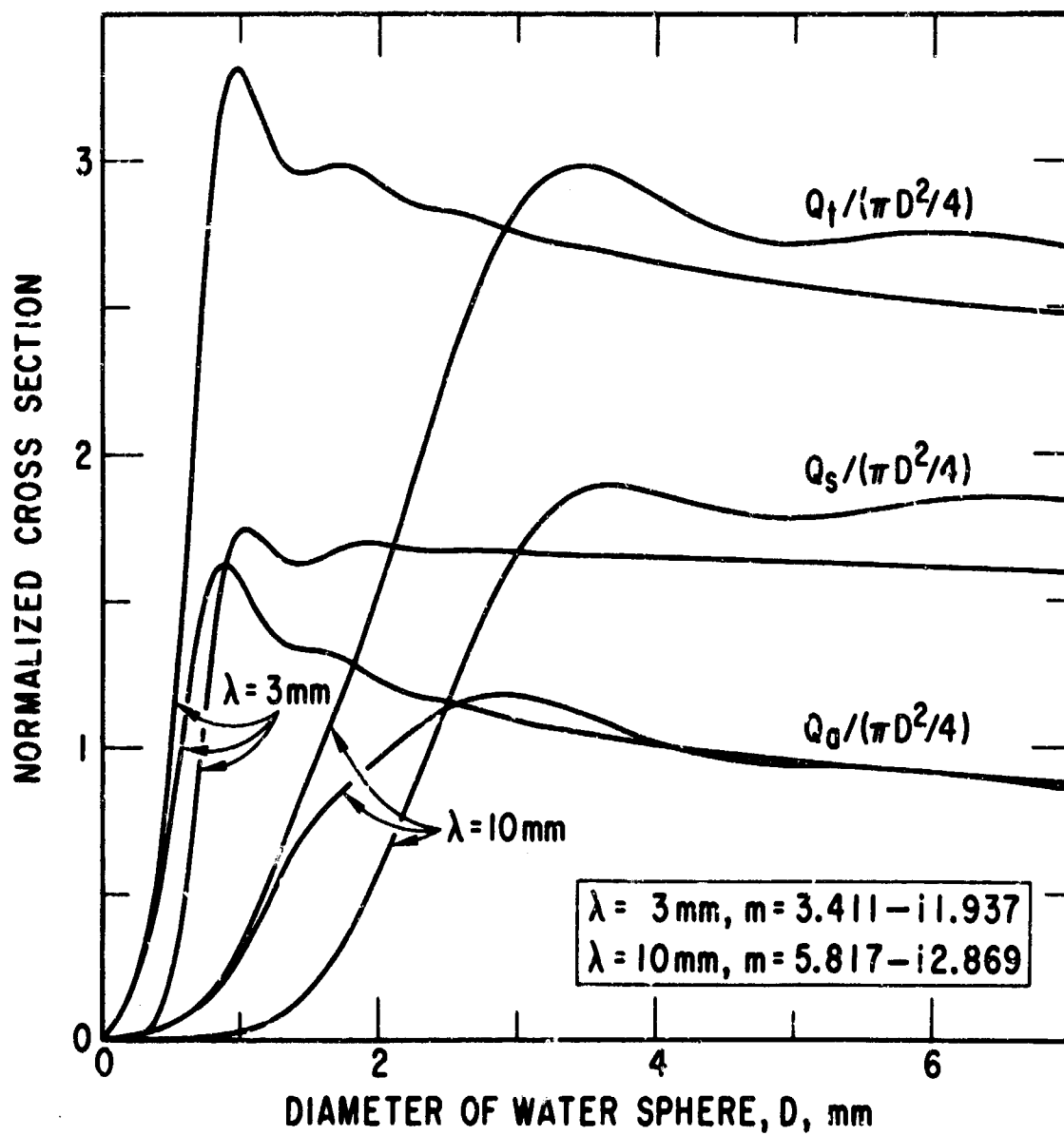


Fig. 7. Absorption, Scattering, and Total Attenuation Cross Sections of Water Spheres

small D/λ (Rayleigh region), scattering and absorption are minimal relative to the regime in which D is comparable to or greater than λ . Particle effects are more significant at millimeter wavelengths than at longer radio wavelengths because of the larger values of D/λ .

The largest atmospheric particles occurring in abundance are raindrops, and these cause the most significant attenuation. Both the size distribution and the density of these particles are dependent on the rainfall rate. Size distribution as a function of rainfall rate is shown in Figure 8 [3]. Attenuation as a function of rainfall rate as calculated using the Laws and Parsons model for drop size distributions is shown in Figure 9. It is readily apparent that even at moderate rainfall rates attenuation is significant at millimeter wavelengths. It would be tolerable, however, for moderate distances and light rainfalls [4]. It should be noted that long path lengths (> 5 n mi) through heavy rain are improbable, even at low elevation angles.

Attenuation due to fog and clouds is also significant at millimeter wavelengths. Although fog and cloud water droplets are typically much smaller than raindrops (D/λ in the Rayleigh region), they are much more dense. In heavy fog (30-m visibility), attenuation is of the order of 1 dB/km at $\lambda = 12$ mm. At shorter wavelengths higher values prevail. Figure 10 [2] shows the attenuation by clouds and fog as a function of wavelength and M , the liquid water content in g/m^3 . In heavy fog, M may be as high as 3 g/m^3 .

Ice particles in clouds or fog attenuate less than water droplets of comparable size and are less numerous. Dry snow or hail attenuates less than rain for the same water content while wet snow attenuates more strongly.

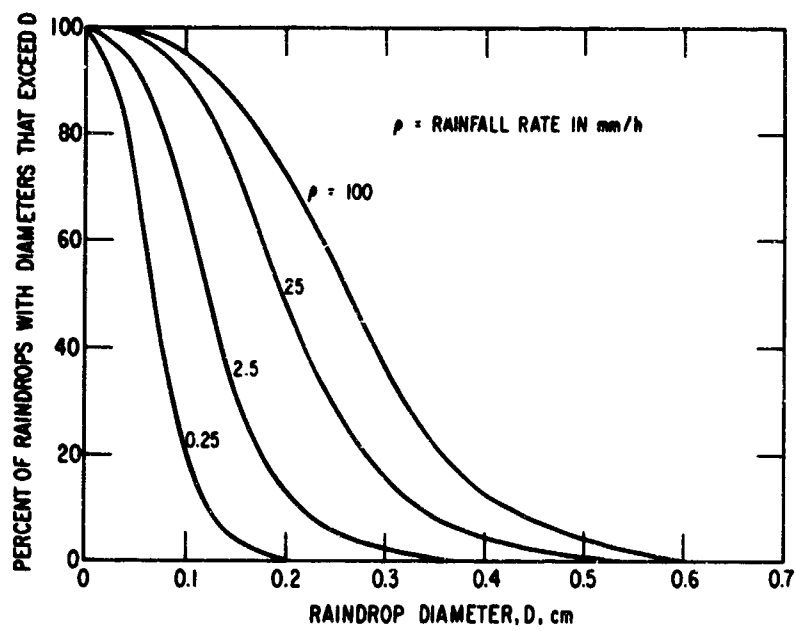


Fig. 8. Size Distribution as a Function of Rainfall Rate

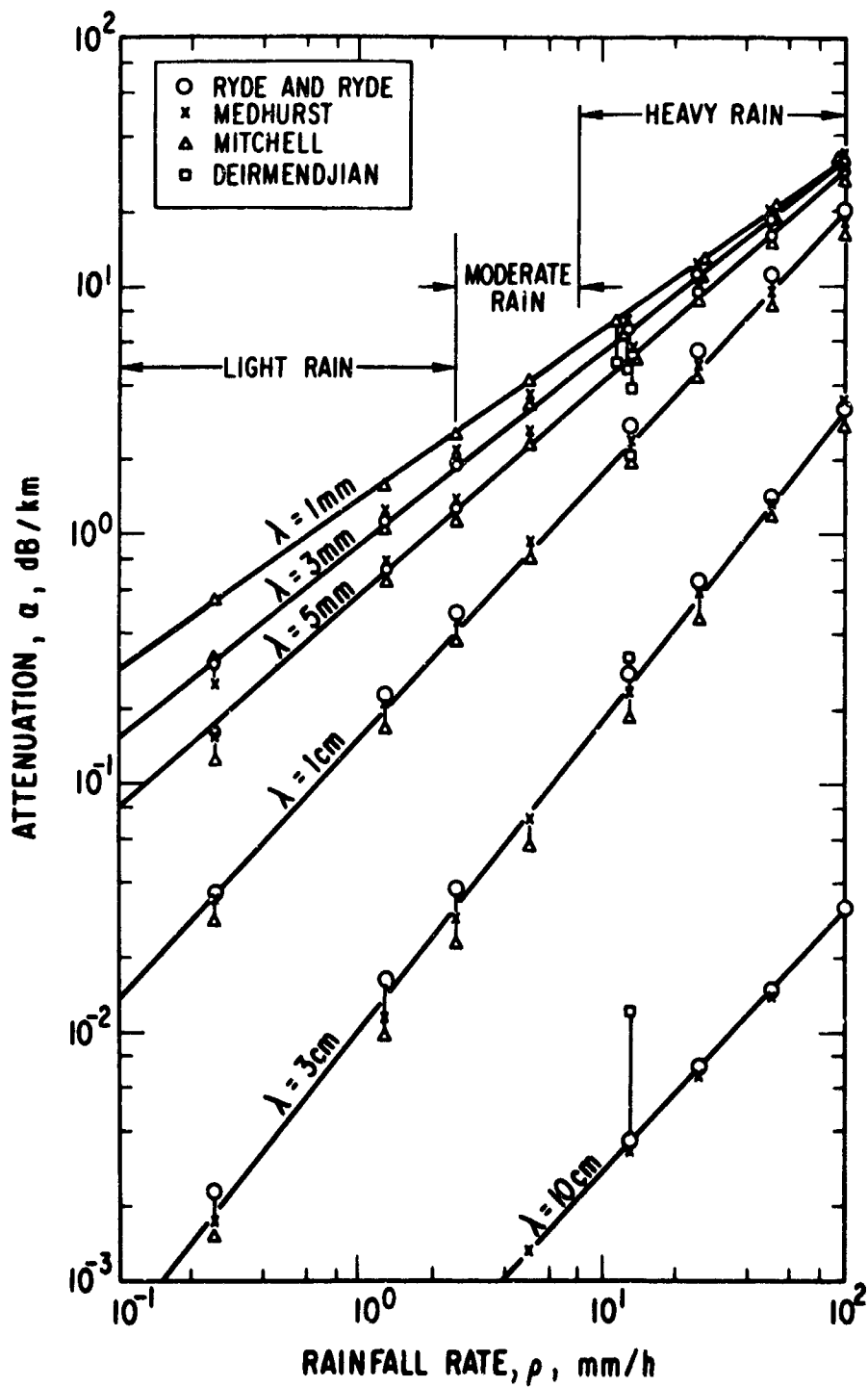


Fig. 9. Theoretical Attenuation vs Rainfall Rate

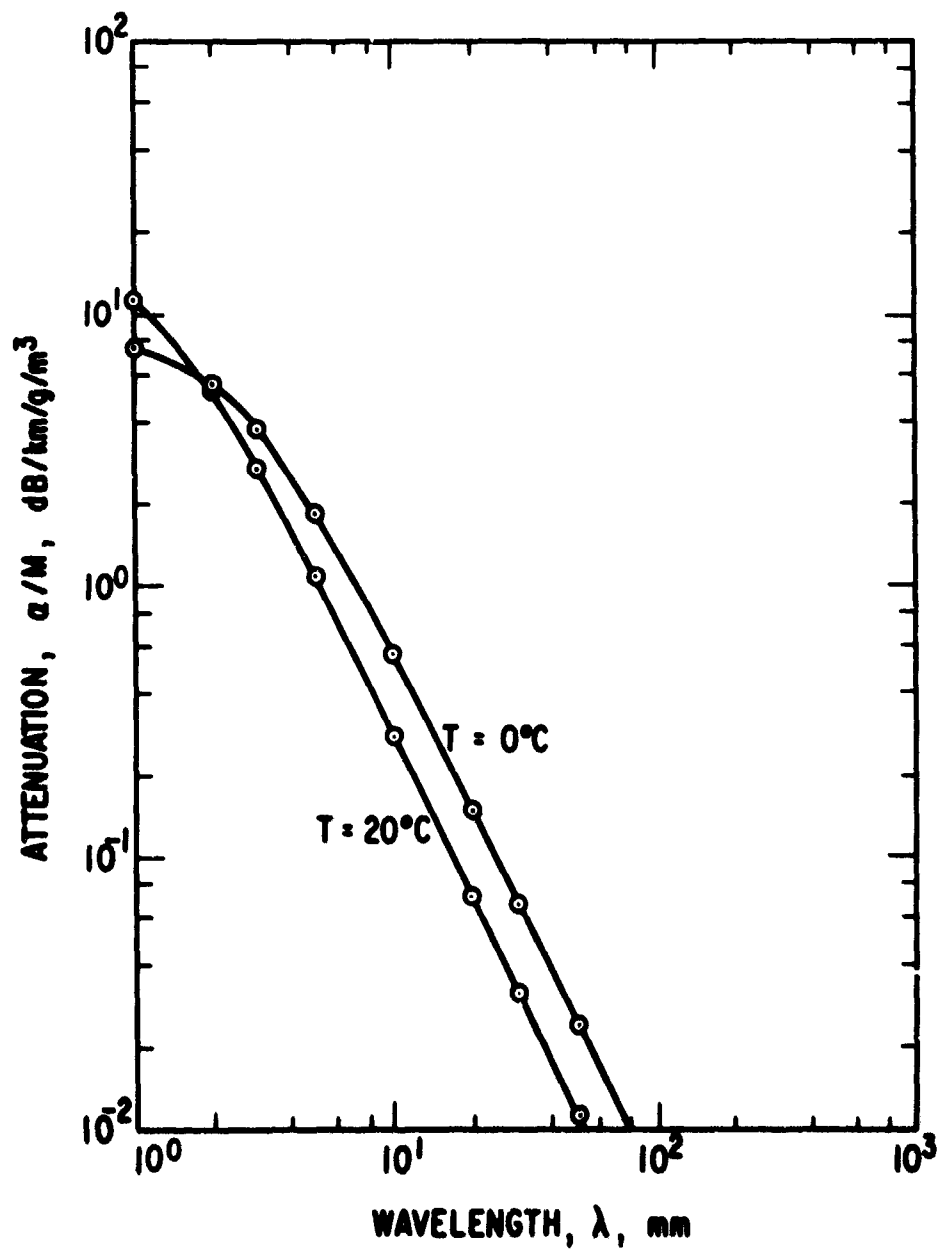


Fig. 10. Attenuation in Clouds and Fog

Aerosols, in general, are much smaller than water droplets and are not a significant factor in millimeter wave propagation. They are numerous, however, and backscatter from aerosols should be detectable with millimeter wave radiation, particularly in maritime air masses where giant salt nuclei are prevalent [2].

B. MOLECULAR RESONANCE ABSORPTION

Molecular oxygen (O_2) and water exhibit numerous resonances in the millimeter- and submillimeter-wavelength regions. The atmosphere is highly absorbent at these resonant frequencies. At sea level, the absorption spectral lines exhibit a large amount of pressure broadening [5], Figure 11. As a consequence, the wings of the lines overlap to provide a residual loss in the intervals between lines. The line sharpening with altitude is indicated by the lower curve in Figure 11. At very high altitudes, the individual lines are completely separated, with negligible attenuation in the intervals or windows between them. The major oxygen absorption at 5 mm then is resolved into a large number of individual lines. Toward shorter wavelengths and into the adjacent far infrared (FIR) region, water vapor lines become very numerous.

Molecular absorption profoundly influences the utility of the millimeter spectrum for communications and other applications. The "windows" between absorption lines provide the only usable portions of the spectrum for propagation over appreciable distances at sea level. At low altitudes, the useful bands are in the 35-GHz and the 70- to 100-GHz regions. At high altitudes, the available spectrum is greater with virtually the entire spectrum usable for paths entirely above 5 km. For communication systems, an

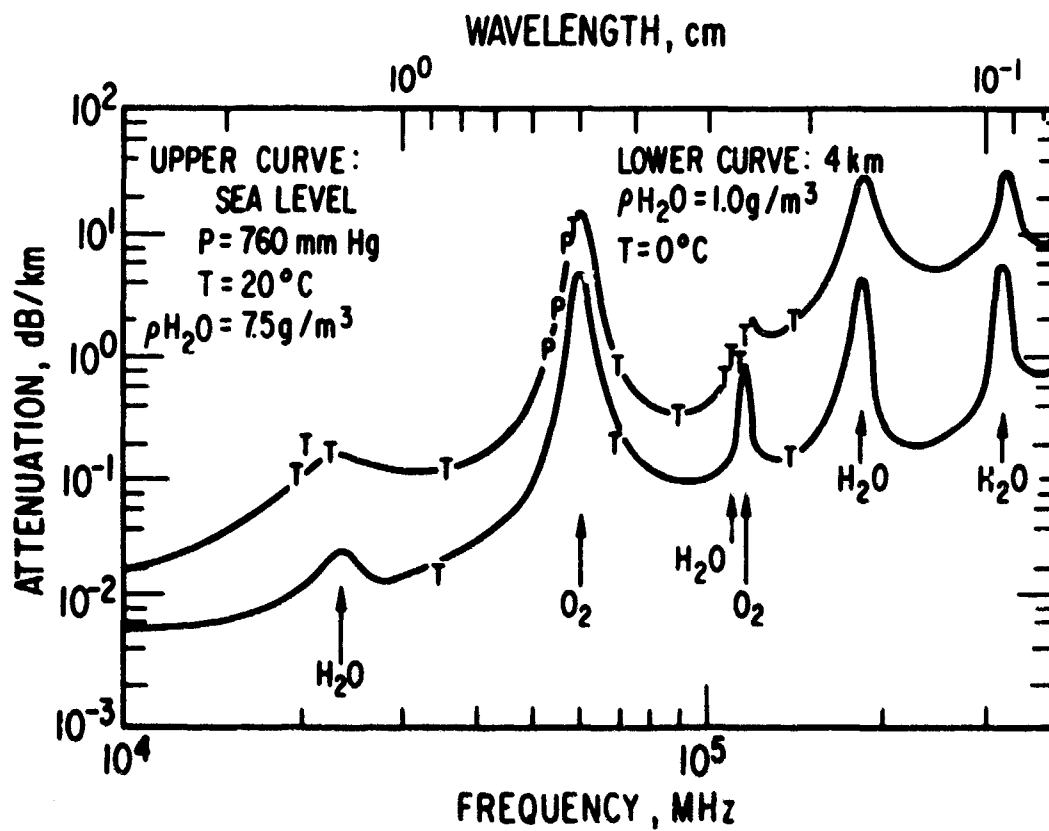


Fig. 11. Attenuation per Kilometer for Horizontal Propagation (From Ref. 5)

additional possibility exists at high altitudes. Where freedom from ground interference, security from ground intercept, or both are desired, a frequency near an absorption line may be chosen. At the operating altitude and above, molecular absorption will then be below a prescribed level, while the attenuation on any path to the ground will be high due to the additional absorption associated with line broadening at the lower altitudes.

For vertical paths through the atmosphere, the total absorption in the spectral windows is quite low, Figure 12 [5]. The data here are a composite of many sources and tend to show greater attenuation than some recent measurements. The technique of vertical measurements relies on the sun (or the moon) as a source. The observed brightness temperature at a zenith angle is

$$T_B = T_s e^{-\alpha \sec z}$$

where T_s is the source brightness temperature, and α is the zenith attenuation in nepers. On taking the logarithm

$$\ln T_B = \ln T_s - \alpha \sec z$$

it is readily seen that a plot of the log of received signal power vs $\sec z$ has a slope $-\alpha$. Typical $\ln T_B$ vs $\sec z$ plots are shown in Figure 13. Variations in humidity are the primary cause of day-to-day changes in attenuation, Figure 14.

The atmospheric absorption of millimeter waves not only attenuates the desired signal but also introduces thermal noise. The resultant equivalent noise temperature or sky background temperature T_g may be computed from

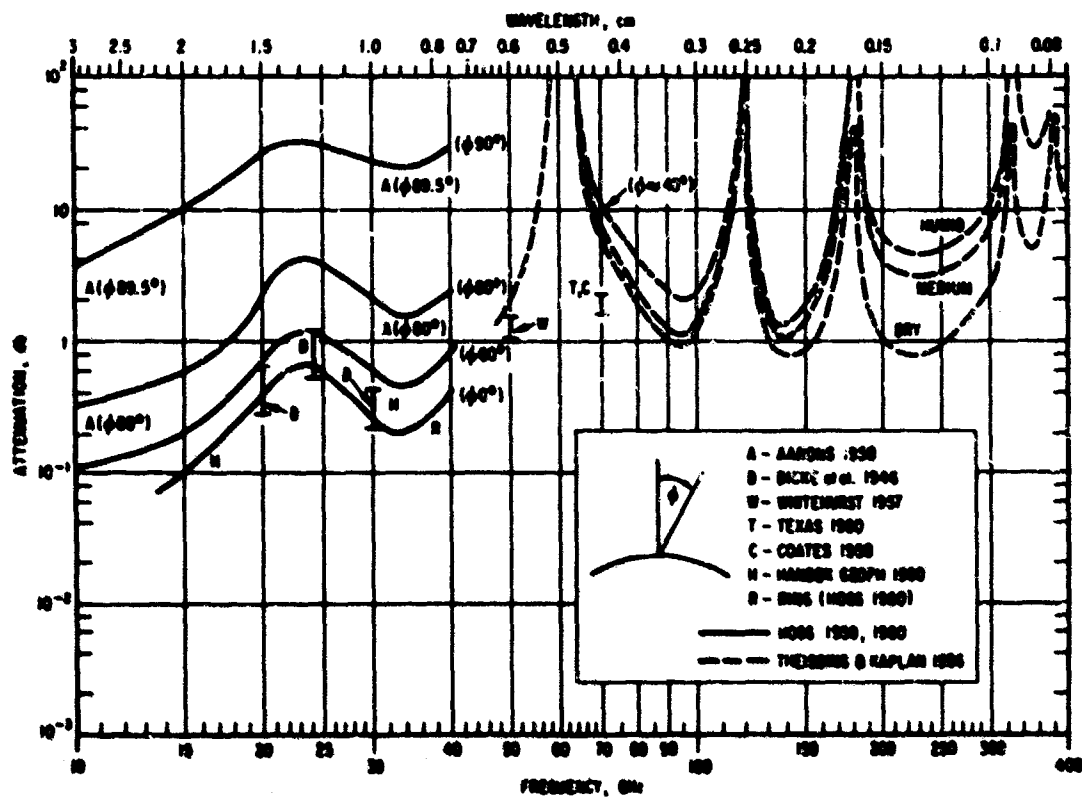


Fig. 12. Total Attenuation for One-Way Transmission Through the Atmosphere (From Ref. 5)

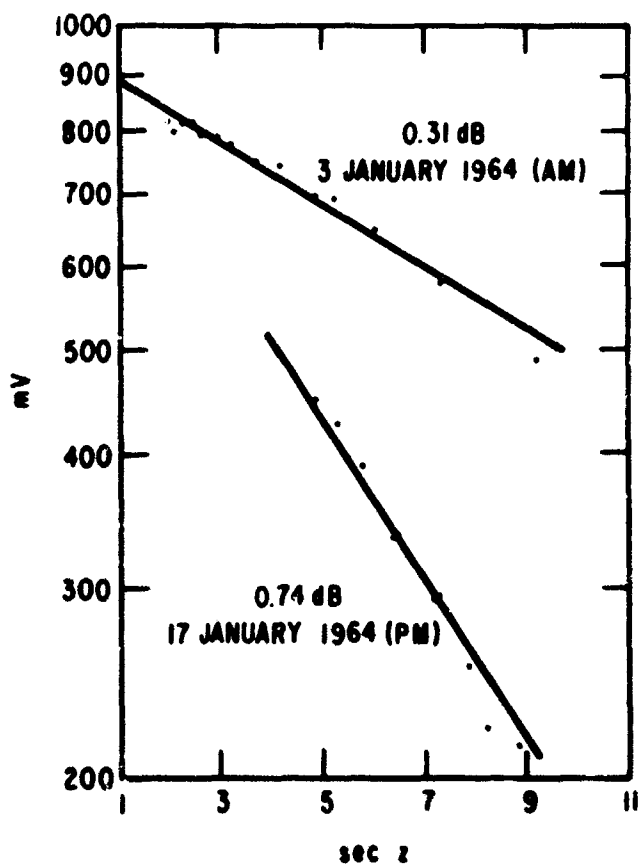


Fig. 13. Atmospheric Attenuation Observations

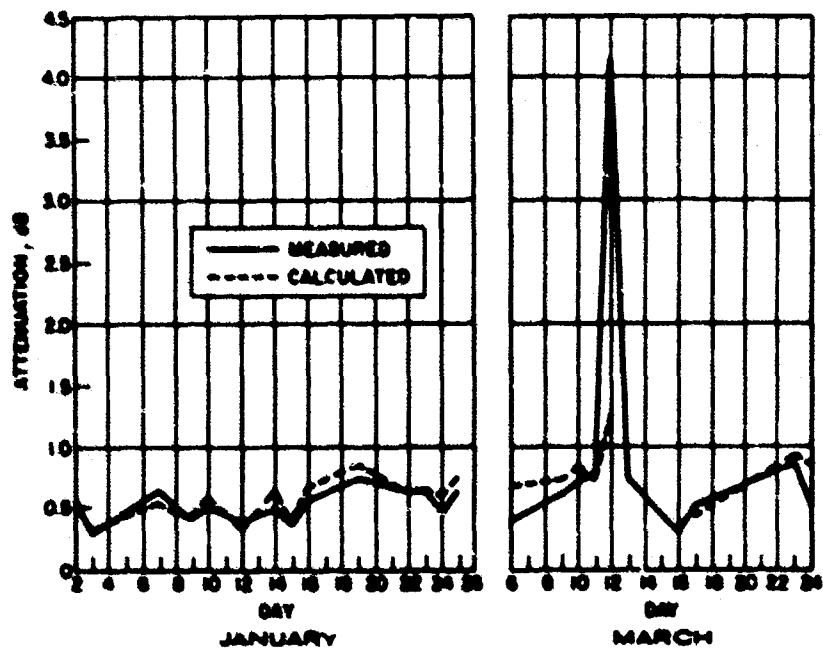


Fig. 14. Day-to-Day Variations in Attenuation

the radiative transfer equation [6]

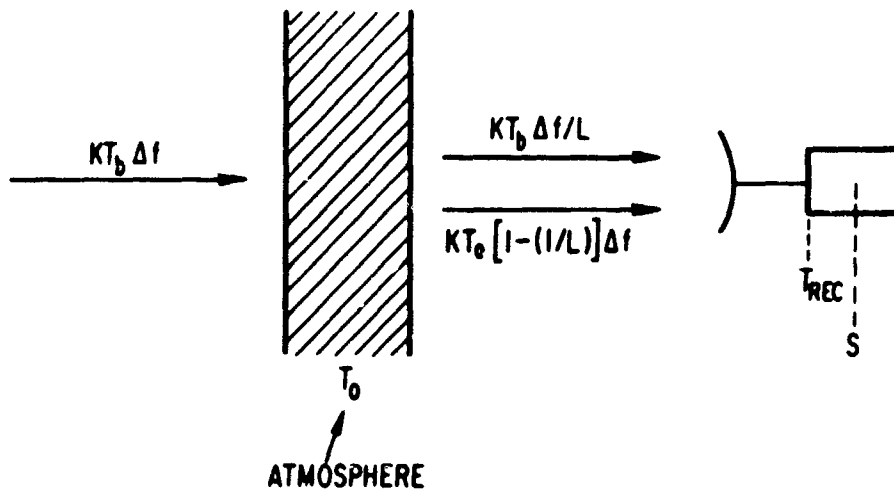
$$T_s = \int_0^\infty T(s) \gamma(s) e^{-\int_0^s \gamma(u) du} ds$$

where s is distance along the transmission path, and $T(s)$ and $\gamma(s)$ are, respectively, the temperature and absorption coefficient at a point on the path. The process is more readily understood if it is assumed that the atmosphere is at a uniform temperature T_0 and has an overall loss factor L . Suppose an antenna is looking at an extraterrestrial blackbody at temperature T_b through an absorber (the atmosphere), Figure 15. The available power incident upon the absorber is $KT_b \Delta f$ where K is Boltzmann's constant, and Δf is the receiving system bandwidth. $KT_b \Delta f / L$ of this power is available at the antenna after transmission through the atmosphere. The emissivity of the atmosphere is equal to its absorption coefficient (the fraction of total power absorbed), $\left[1 - \left(\frac{1}{L}\right)\right]$. Hence the atmosphere is a thermal source presenting available power $KT_0 \left[1 - \left(\frac{1}{L}\right)\right] \Delta f$ to the antenna. Thus, the crude uniform atmosphere model yields for the sky background temperature

$$T_s \approx T_0 \left[1 - \left(\frac{1}{L}\right)\right]$$

For example, an ambient temperature $T_0 = 290^\circ\text{K}$ and an absorption loss of 2 dB yield a background temperature of 107°K . The receiver sensitivity or noise level is

$$S = K(T_{\text{receiver}} + T_{\text{antenna}}) \Delta f$$



$$S = K(T_{\text{RECEIVER}} + T_{\text{ANTENNA}}) \Delta f$$

$$(T_{\text{ANTENNA}})_{\text{min}} = T_0 [1 - (1/L)]$$

Fig. 15. Uniform Atmosphere Model

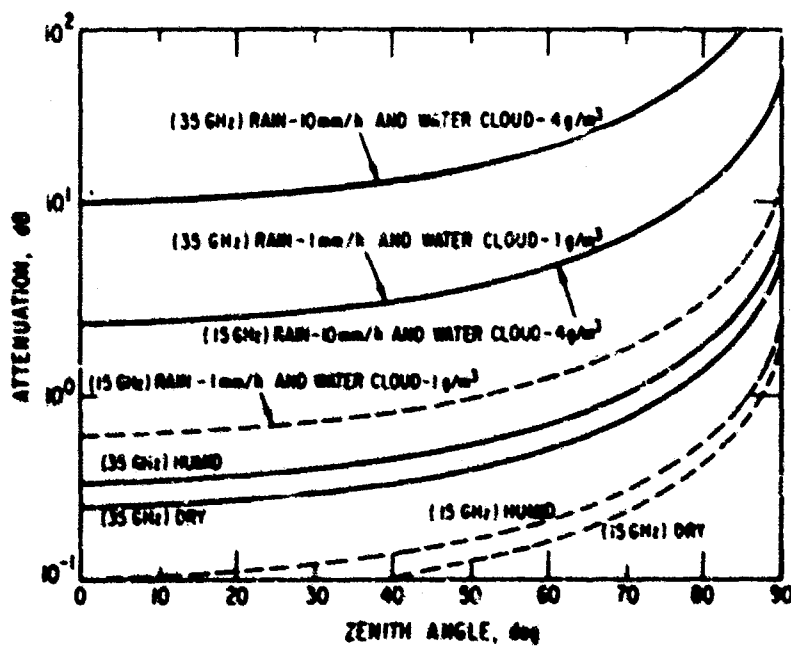


Fig. 16. Attenuation of a Stratified Atmosphere

T_g represents a lower limit for antenna noise temperature, which is generally augmented by unwanted extraterrestrial sources and local emitters in the antenna sidelobes. It is apparent that little is gained by seeking receiver noise temperatures far below the antenna temperature. For low elevation angle paths in the atmosphere, the sky background noise temperature approaches ambient temperature.

C. TOTAL ATMOSPHERIC ATTENUATION

The various contributors to atmospheric attenuation are not uniformly present over any propagation path. This is particularly apparent for an earth-to-space communication link. The collective effects for a stratified atmosphere are shown in Figure 16 for two frequencies at the long wave end of the millimeter spectrum [7]. The drastic increase in total attenuation at zenith angles near 90 deg reflects the long path through the lower atmosphere, which contributes virtually all of the loss; it is about 6-km thick at zenith, but near horizon angles, some 170 km of lower atmosphere is traversed.

For practical satellite communications, the low elevation angles are of primary importance. This is illustrated on consideration of the visibility time for a satellite in a circular orbit at an altitude of 300 mi, as shown in Figure 17 [7]. Figure 18 shows that increasing the satellite altitude improves the situation only slowly [7]. These results are good approximations for moderately elliptical orbits as well.

D. REFRACTIVE EFFECTS

The index of refraction of the atmosphere in the microwave region is given by the Smith-Weintraub equation [8]

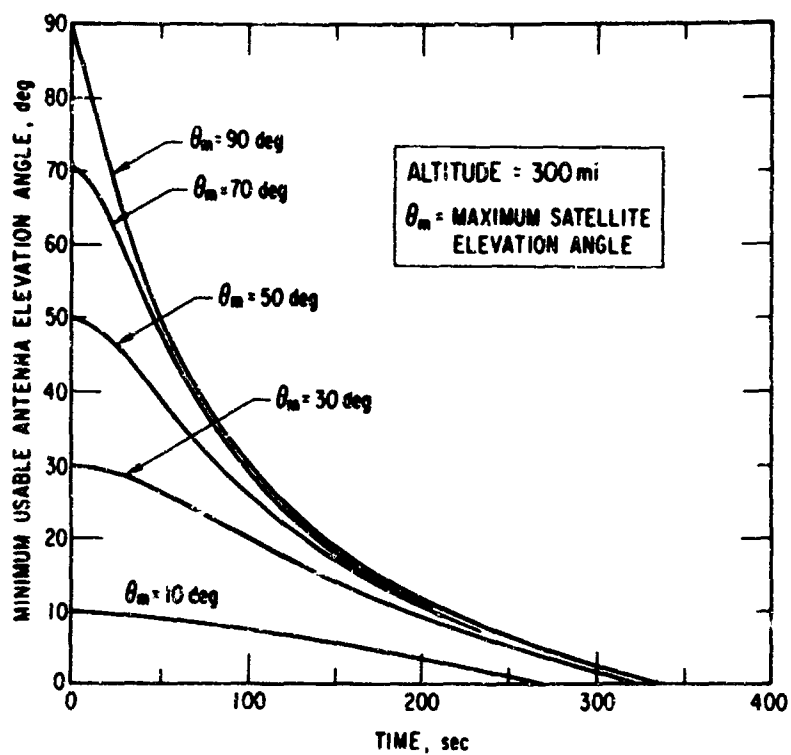


Fig. 17. Visibility Time vs Minimum Antenna Elevation Angle and Maximum Satellite Elevation Angle

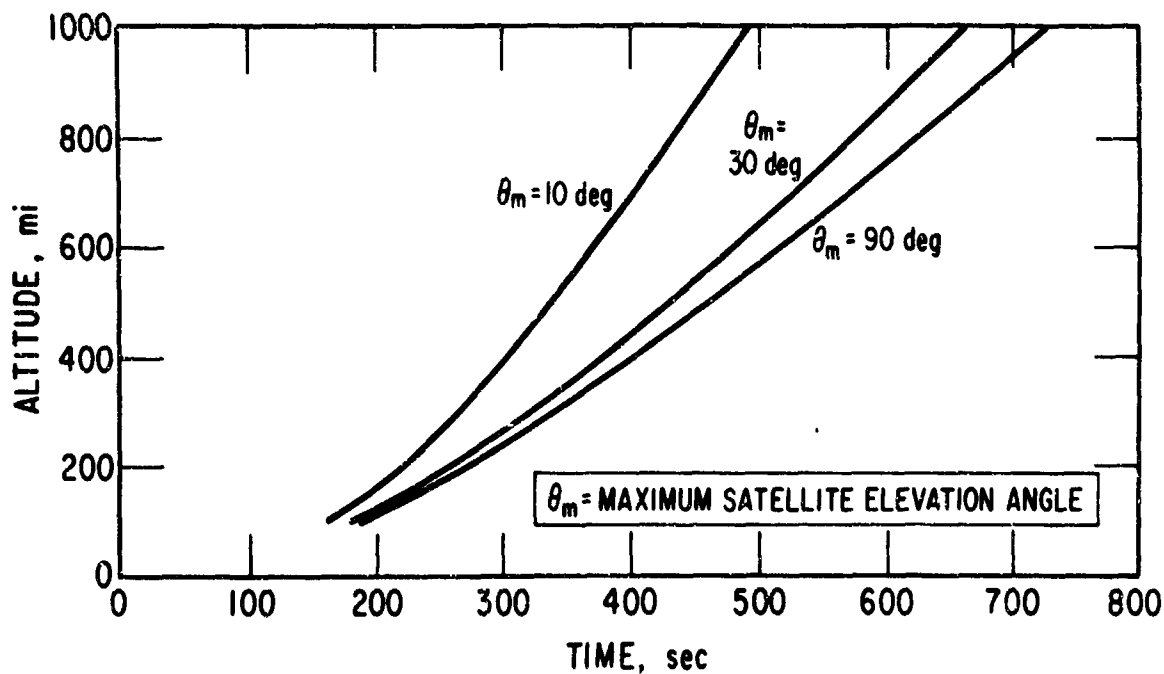


Fig. 18. Visibility Time vs Satellite Height and Maximum Elevation Angle

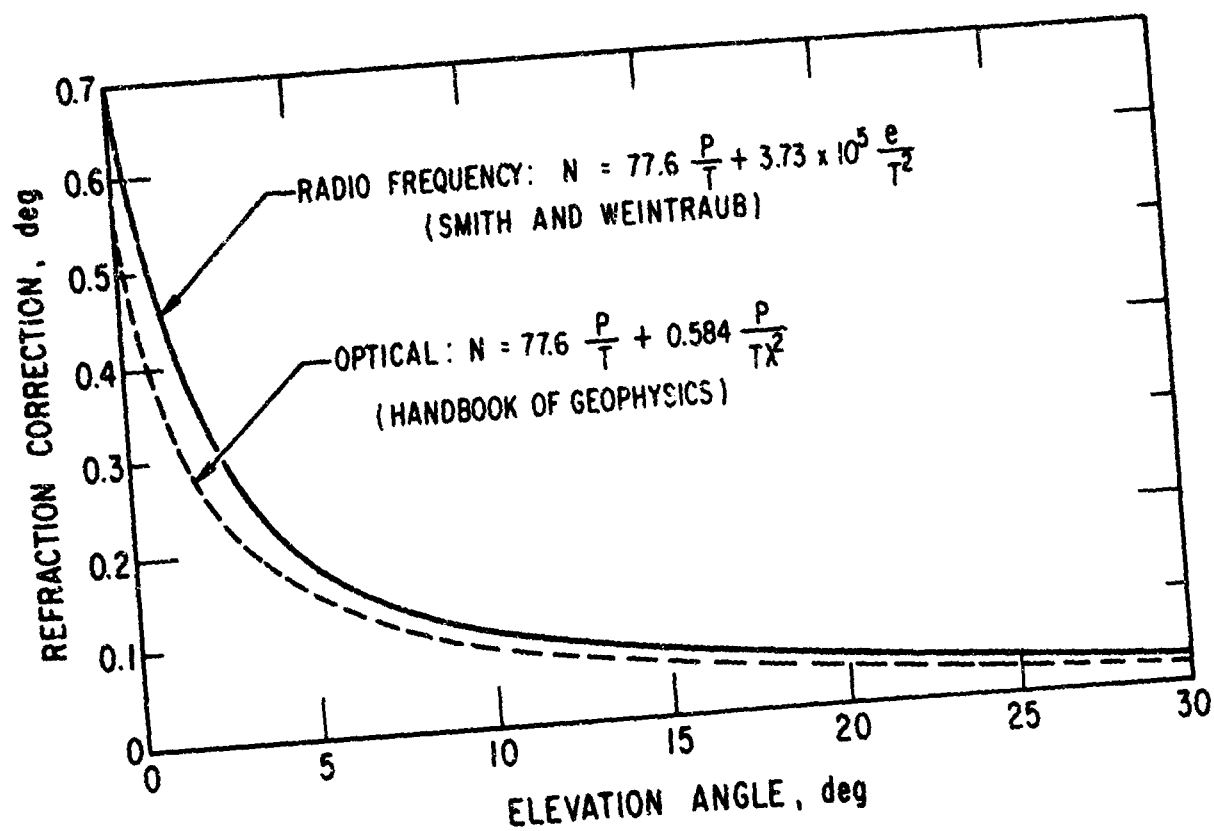


Fig. 19. Atmospheric Index of Refraction Corrections

$$N = 77.6 (P/T) + 3.73 \times 10^5 (e/T^2)$$

where

$$N = (n-1)10^6,$$

n = index of refraction

P = pressure, mbar

e = partial pressure of water vapor, mbar

T = temperature, °K

An angle-of-arrival correction can be computed for waves traversing the atmosphere. The basis for the computation is the above equation and a standard atmosphere specifying the gross variations in P , e , and T . Such a correction and its optical counterpart are shown in Figure 19. The increased correction for microwaves relative to optical frequencies is due to the presence of water vapor in the standard atmosphere for which the curves were drawn. For perfectly dry air, the index is the same for optical and microwave frequencies. For narrow beam antennas, the gross angle of arrival correction is important, and it is characteristically made in radio location measurements.

In addition to the smooth predictable variation in index of refraction that results when the Smith-Weintraub equation is applied to a standard atmosphere, there are small random variations attributable to atmospheric turbulence. The effect of these random fluctuations is particularly familiar in optics in the twinkling of stars and the dancing of images viewed through hot air drafts above chimneys. Waves propagating through regions of atmospheric turbulence have the equiphase surfaces distorted; their amplitudes become randomly modulated. Both effects are described by saying that the waves lose their spatial coherence [9].

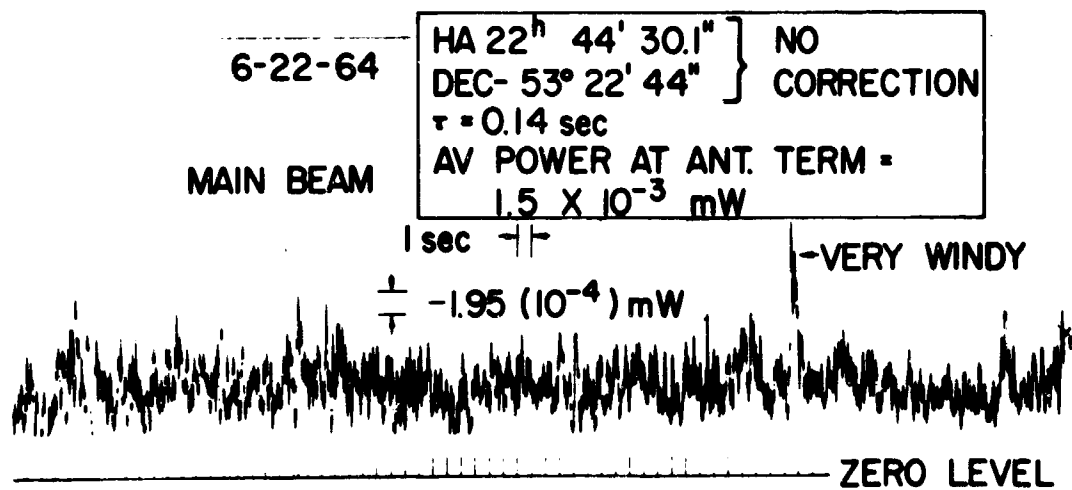


Fig. 20. Scintillation of Main Beam Power

The distance (normal to the direction of propagation) over which spatial coherence extends after propagation through the atmosphere determines the angular resolution attainable in radio measurements. For example, at optical frequencies, this distance is typically of the order of 1 ft, and 1-ft-diam optical telescopes have essentially maximum resolution. Larger telescopes are practicable, but only because of their increased light-gathering power, e.g., the 200-in. Mt. Palomar telescope.

At radio frequencies, adequate spatial coherence is maintained over much greater distances, since the small-scale wavefront perturbations that can blur optical images are negligible in comparison to radio wavelengths. The distance is large enough so that beam broadening (the equivalent of image blurring in optics) is not commonly observed with practical radio antennas. It is however, observable with radio astronomy antennas of large aperture-to-wavelength ratios [10]. Two effects are observed: (1) beam broadening due to wavefront perturbations of spatial extent is small compared to the aperture, and (2) wavefront tilt or angle of arrival scintillation associated with larger wavefront perturbations [11]. The two effects are indistinguishable after long time averaging, but are to some extent separable since the tilt fluctuations are slower in time. Thus, best resolution is obtained with short observation times. These effects at millimeter-wave frequencies are shown by the accompanying figures. Figure 20 is a plot of the fluctuations in power received on a 15-ft antenna from a 3.2-mm point source at a distance of 10 n mi. The fluctuations are due to (1) actual amplitude scintillation of the arriving wavefronts, and (2) amplitude modulation introduced by the tilting of the 2.78-arc-min beam relative to the

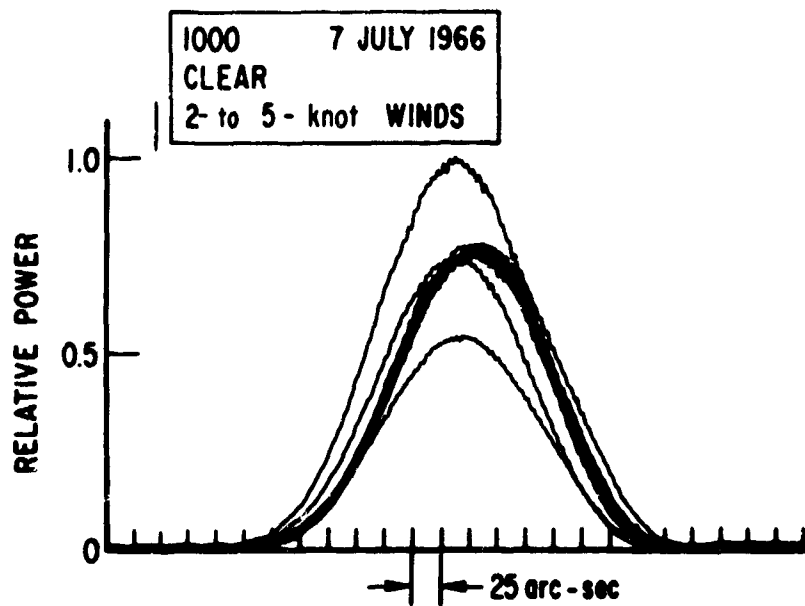


Fig. 21. Superposed Antenna Patterns,
Turbulent Atmosphere

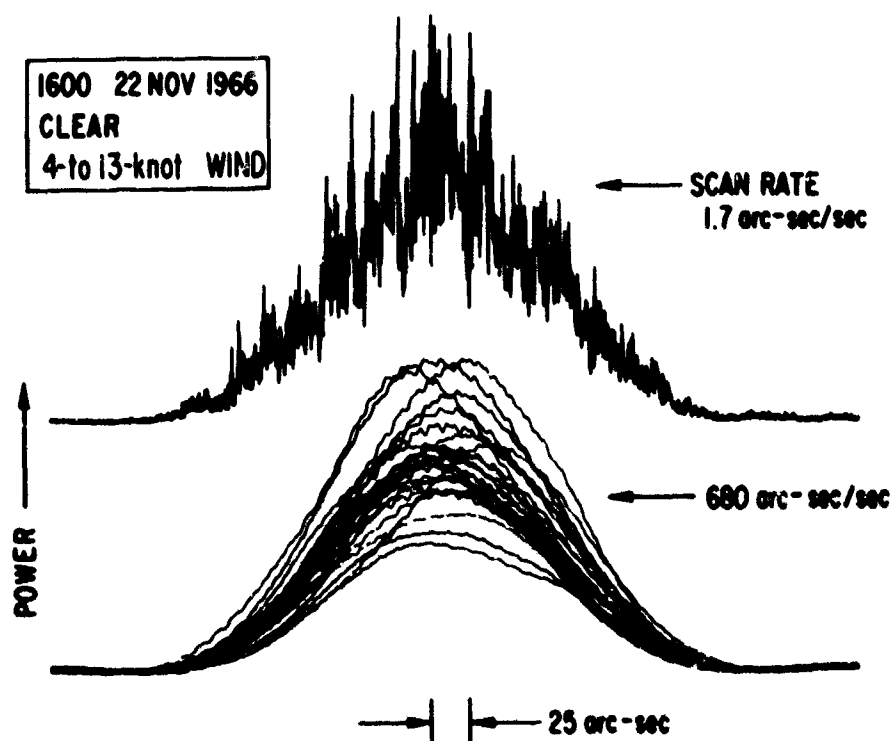


Fig. 22. Slow and Rapid Scan Antenna Patterns,
Turbulent Atmosphere

direction of the point source. Figure 21 shows the power pattern obtained when the receiving antenna is scanned rapidly past the point source [12]. Repetitions of the same scanning motion show the beam position change associated with atmospheric turbulence. This position change is random and may be quite significant for a clear turbulent atmosphere. Figure 22 shows the power pattern obtained when the receiving antenna is scanned very slowly [12]. The contrast with the rapid scan patterns clearly demonstrates the loss of resolution in long time averaging.

Measurements of spatial coherence with the 15-ft antenna and a 27-ft-baseline interferometer suggest that the angular resolution potential of antennas at least as large as 40 ft may be utilized despite the atmospheric limitations. It may be possible to extend the atmospheric resolution limit even farther by compensation, as with a fast response tracking antenna that eliminates the effect of wavefront tilt or with a transmitted reference wavefront that functions in a manner analogous to that of the carrier in a phase-lock loop communications link.

In addition to limiting angular resolution, atmospheric turbulence introduces phase and amplitude noise on transmitted signals. This may be limiting in certain applications, but, fortunately, it is limited to very low frequencies (essentially less than 1 kHz at 3 mm).

E. SIGNIFICANT OBSERVATIONS

The most significant aspects of millimeter-wave propagation through the atmosphere are:

1. Absorption and scattering from rain drops make long paths prohibitively lossy.
2. Molecular resonance absorption limits the useful spectrum to windows between absorption lines. At high altitudes, narrow lines permit low-loss propagation isolated from ground level.
3. The sky background temperature in the millimeter region is between 30°K and ambient, depending on the elevation angle and frequency.
4. Gross refractive effects can be predicted using a standard atmospheric model, but random scintillation due to atmospheric turbulence sets a limit on useful beamwidths.

III. STATE OF THE MILLIMETER-WAVE ART

A. ANTENNAS

The Aerospace 15-ft-diam antenna is shown in Figure 23; its characteristics are outlined in Figure 24. The antenna became operational 22 December 1963 at a frequency of 94 GHz (3.2 mm). The first planned observation was the lunar eclipse event of 30 December 1963. One result of these observations was the detection, for the first time, of temperature decreases on specific lunar areas (i.e., mountainous areas, plains, and specific crater complexes) as the eclipse progressed. Of course, there is a great temperature change at infrared (IR) wavelengths, but none had been detected before on identifiably different types of lunar areas at radio wavelengths.

This antenna has one of the largest diameter-to-operating-wavelength ratios (figure of merit related to gain) (Figure 25), and its efficiency is remarkably high. Preliminary measurements indicate that the antenna efficiency is about 35% at 1.4 mm (210 GHz). The 36-ft-diam NRAO antenna at Kitt Peak National Observatory possesses similar observational capabilities; it is theoretically better by about 8 dB above 2mm, this difference falling to 4.5 dB at 1 mm.

B. POWER SOURCES

The power output capabilities of millimeter-wave tube devices are summarized in this section, principally to identify the most common and useful sources of millimeter-wave power and to serve as a systems planning guide for radar and communications engineers. The tube sources considered are

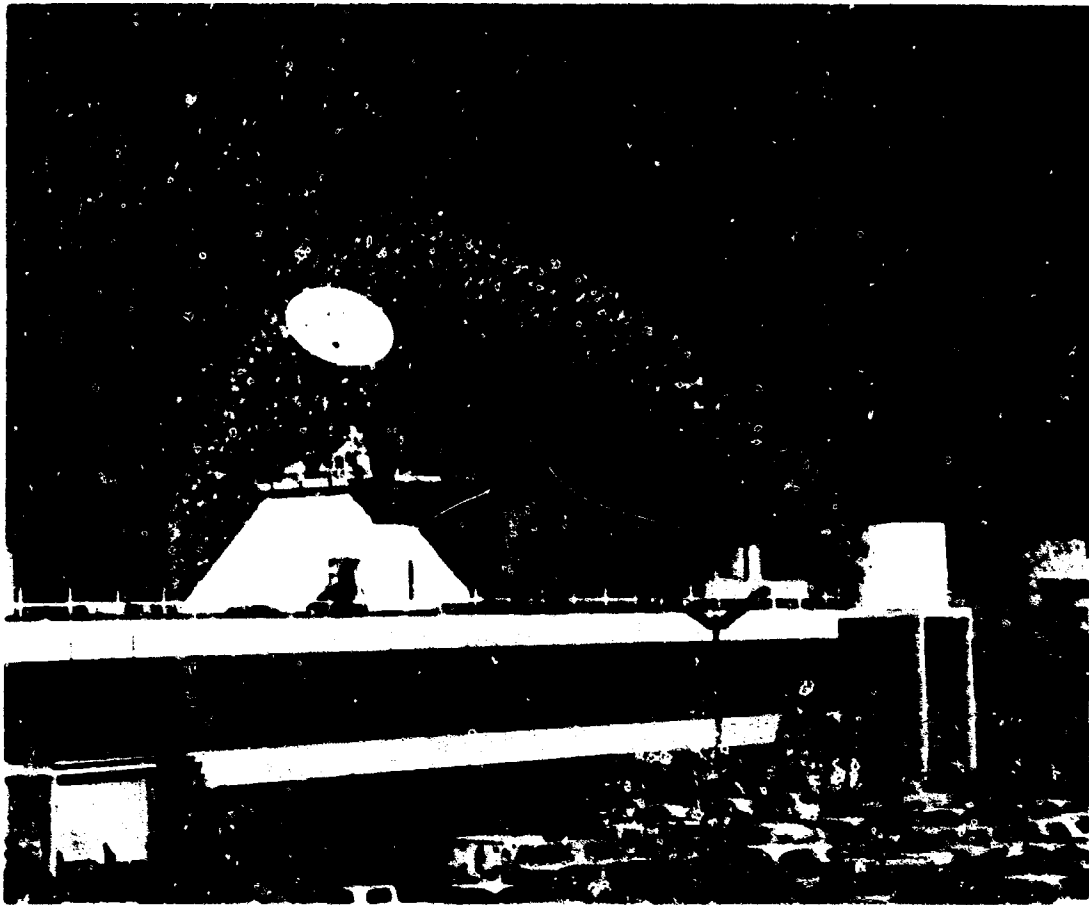


Fig. 23. The 15-ft Antenna

- GAIN (94 GHz) _____ 70 dB
- BEAMWIDTH (3dB, 94 GHz) _____ < 3 arc-min (0.05 deg)
- CONTROL CAPABILITY _____ AUTOMATIC PROG POINTING
- POINTING ACCURACY _____ 20 arc-sec (0.0055 deg)
- TRACKING RATES _____ 0.001 deg/sec TO 3 deg/sec
- OPERATING WAVELENGTH _____ TO 1mm (300 GHz)
- DEVIATIONS FROM TRUE PARABOLA
 - ZENITH _____ 0.00018 IN rms
 - 60 deg FROM ZENITH _____ 0.00031 IN rms
 - 90 deg (HORIZON) _____ 0.0036 IN rms
- SPECIAL FEATURES
 - DEW PREVENTION BY THERMAL HEATING
 - PAINTED REFLECTOR FOR INFRARED SCATTERING

Fig. 24. Characteristics of 15-ft-diam. Antenna

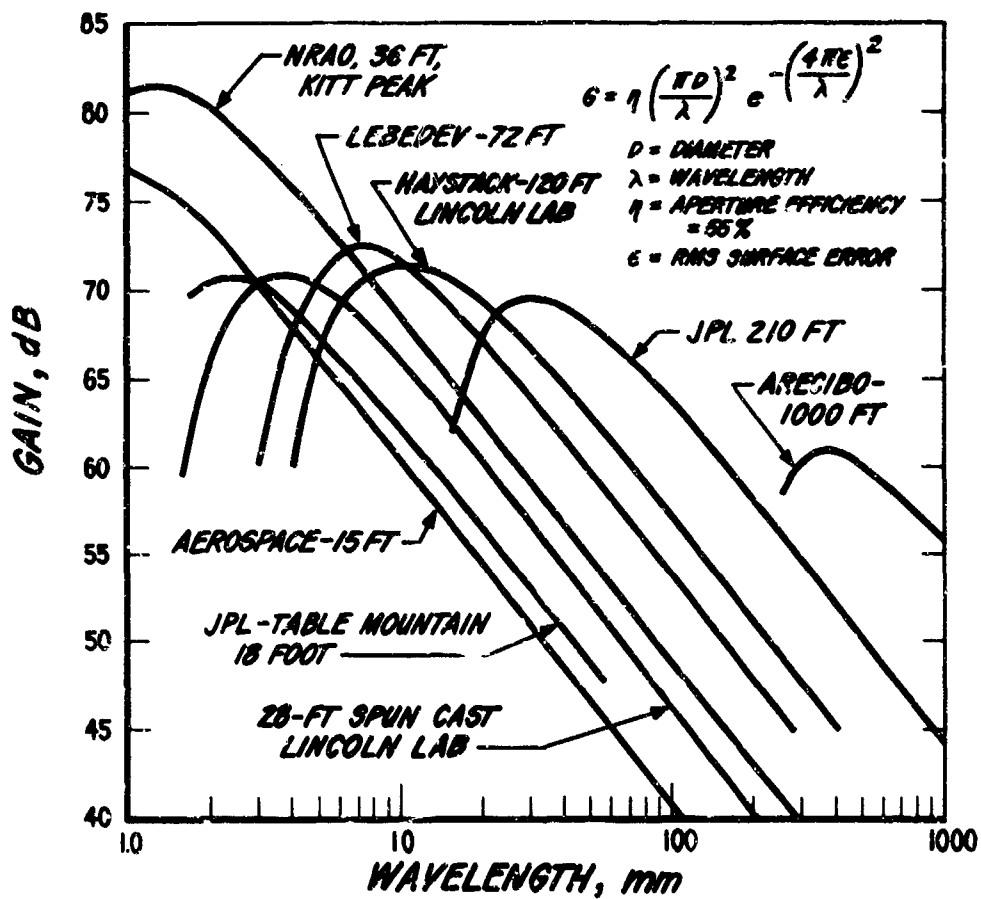


Fig. 25. Gain vs Wavelength Summary for Millimeter-Wave Antennas

classified as klystrons, travelling wave tubes (TWT), or magnetrons. The CW power output capabilities for reflex klystrons, floating drift tubes (two-cavity klystrons), backward wave oscillators (BWO), and travelling wave tubes are shown in Figures 26 through 29. The pulse power-output capability of magnetrons is shown in Figure 30. The figures estimate production model availability and the state of the art for ground-based equipment for the early 1970's.

1. REFLEX KLYSTRONS

The reflex klystron is one of the most important sources of millimeter-wave power known today. The CW power output ranges from about 1 W at 40 GHz to 10 mW at 220 GHz (Figure 26). It is characterized as a low-power CW oscillator. Its useful power output ends in the 200- to 300-GHz region due to limitations imposed by heat transfer in small electrode structures and by excessive beam power density requirements of small diameter electron beams. Reflex klystrons are tunable over fairly large tuning ranges by combined mechanical and electrical tuning. In the millimeter-wave range, typical efficiencies range from 1 to 2%. They are probably the most inexpensive source of millimeter-wave power known today. Single-unit costs range from about \$1500 (40 GHz) to \$9000 (220 GHz). Typical applications include: test sources for component measurements, local oscillators for receivers, and low-power transmitters.

2. FLOATING DRIFT TUBES

In principle, the floating drift tube oscillator is a two-cavity klystron amplifier with a floating drift tube section interconnecting the cavities and a feedback coupling from the output cavity to the input cavity. The tube is

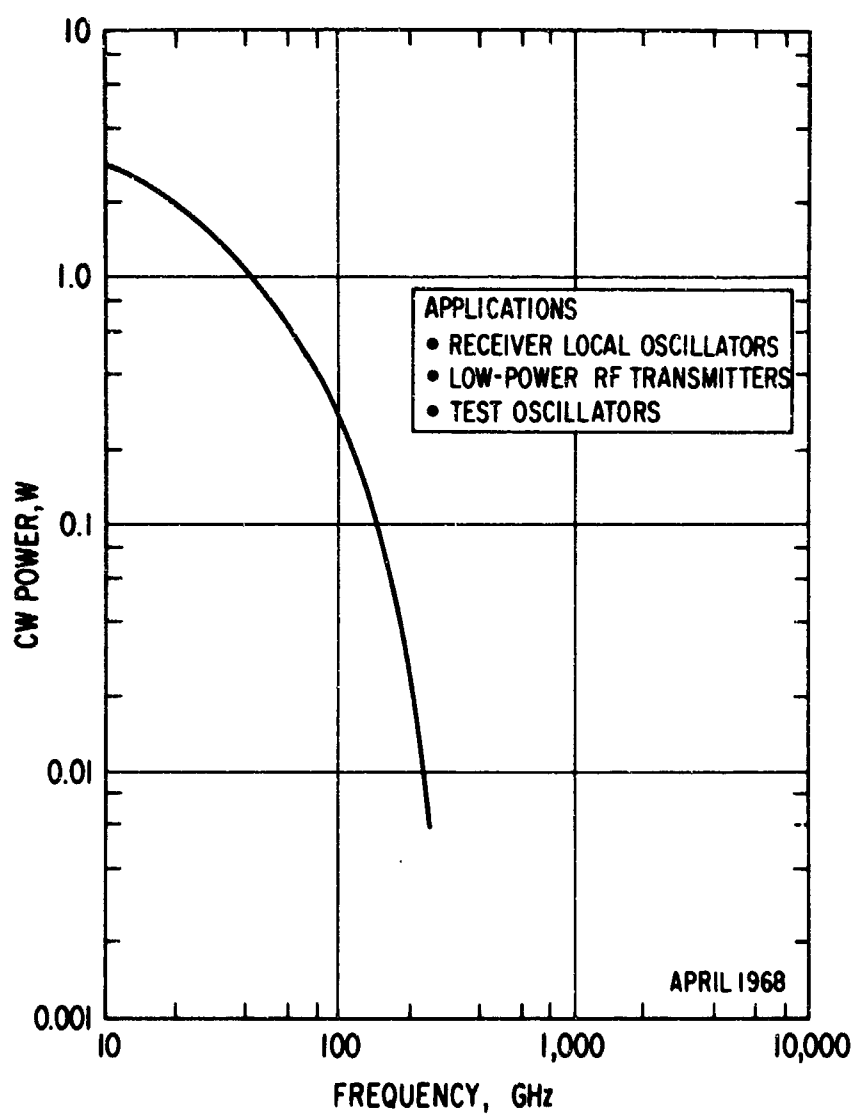


Fig. 26. Reflex Klystrons CW Power Capability
(Production Models - 1970 Estimate)

characterized as an intermediate CW-power oscillator whose power output ranges from about 40 W at 40 GHz to 100 mW at 100 GHz, Figure 27. The useful power output terminates in the millimeter-wave region at about 150 GHz due to the limitations imposed by heat dissipation in small electrode structures and also because of beam divergence problems with high-power electrostatically focused beams. Floating drift tube klystrons are normally designed for operation at fixed frequencies, although small tuning adjustments can be accomplished by mechanical tuning of the coupled cavities. Characteristically, the drift tube klystron is specified for single-frequency operation. The tube structure design produces an extremely low noise output because it minimizes beam interaction and ion oscillations. The drift tube klystron is principally used for applications where a low noise spectrum is required with intermediate power capability. These applications include: ground and air-borne doppler navigation transmitters, doppler radars, and bench-test sources. Frequently they are useful as pump sources for parametric amplifiers.

3. BACKWARD WAVE OSCILLATORS (BWO)

In their basic configuration, BWO's are TWT's in which the energy in the beam and the energy in the slow wave structure are phased to produce continuous positive feedback along their total interaction length. In concept, the distributed feedback supports the oscillations. Backward wave oscillators are capable of producing useful CW outputs well into the submillimeter region. The power-output ranges from about 100 W at 40 GHz in the millimeter-wave region to 1 mW at 620 GHz in the submillimeter-wave region, Figure 28. Octave bandwidth tuning can be achieved on low-power types. Higher power versions are capable

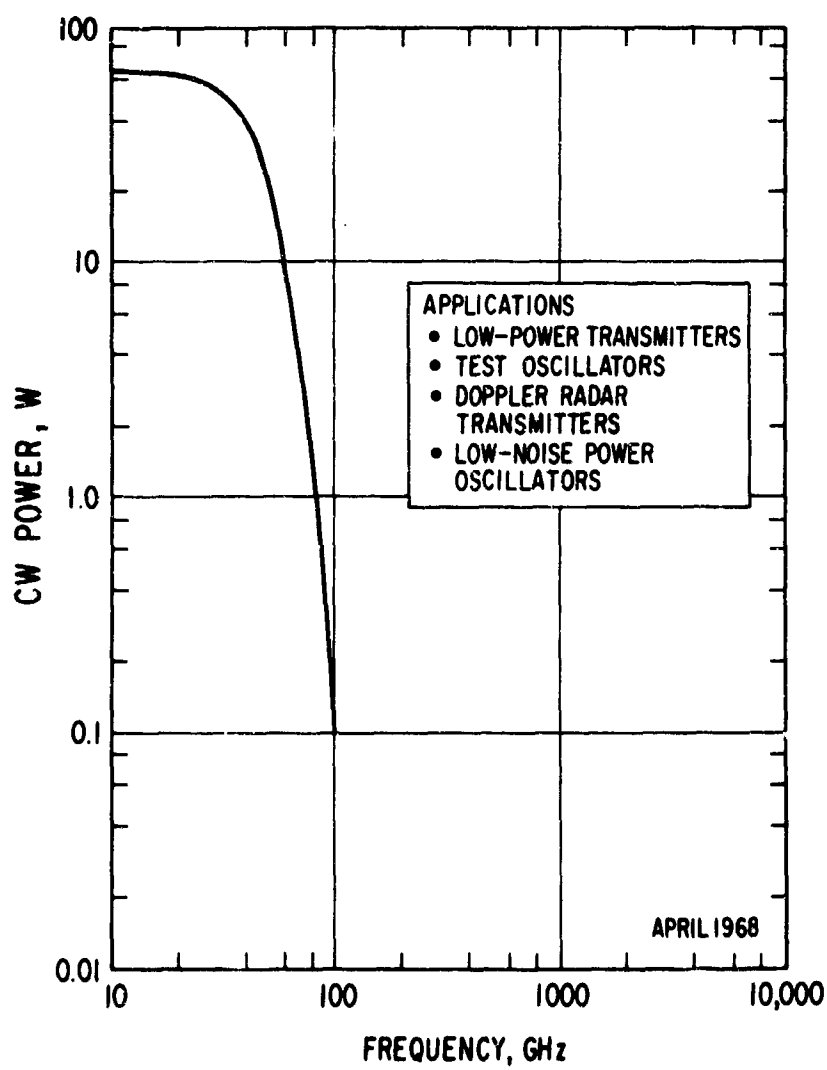


Fig. 27. Floating Drift Tubes (Two-Cavity Klystrons, Laddertrons) CW Power Capability (Production Models - 1970 Estimate)

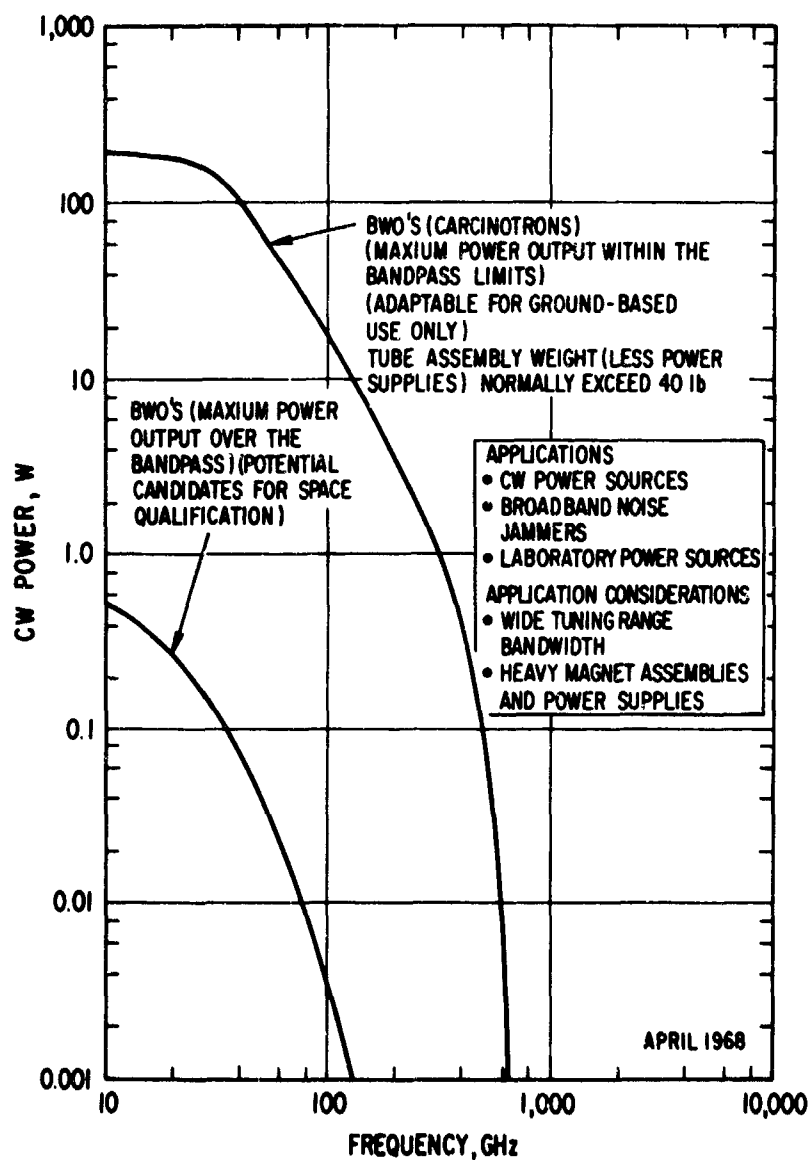


Fig. 28. Backward Wave Oscillators and Carcinotrons CW Capability (State of the Art, 1970)

of rapid frequency tuning (megacycle rates) over 10 to 15% bandwidths. Typical efficiencies approach 30%. With depressed collectors and special circuit designs, efficiencies of 50% can be achieved. Typical applications for BWO's include: wide-band laboratory test sources, wide-band frequency modulated oscillators, and noise-modulated jammer transmitters.

4. TRAVELLING-WAVE TUBE AMPLIFIERS

Millimeter-wave travelling-wave tube amplifiers (TWTAs) are, typically, scaled versions of microwave types. These tubes are presently capable of producing the highest average power at millimeter wavelengths over any other tube device. The CW power-output capability ranges from about 10 kW at 40 GHz to 20 W at 150 GHz, Figure 29. At 94 GHz, a 1-kW TWTAs is commercially available (on special order) for millisecond pulselengths. The bandwidth of high-power TWTAs range from 4 to 10%, depending upon requisite compromises with efficiency, weight, power output, and volume. It should be recognized that a 4% bandwidth at 94 GHz, for example, represents 3.8 GHz of electronic bandwidth — still a truly wide-band device. TWTAs efficiencies range from 10 to 30%. Depressed collectors provide the higher efficiency ratings. Typical applications for TWTAs are as coherent, broadband amplifiers for radar and communications systems.

5. MAGNETRONS

Magnetrons are characteristically employed as sources of high peak power pulses of relatively short duration. The average power must necessarily be low because, in the magnetron electrode configuration, the delicate resonant anode must intercept the total current flow. In the millimeter wavelength region, the size of anode structure diminishes to virtually microscopic proportions, and

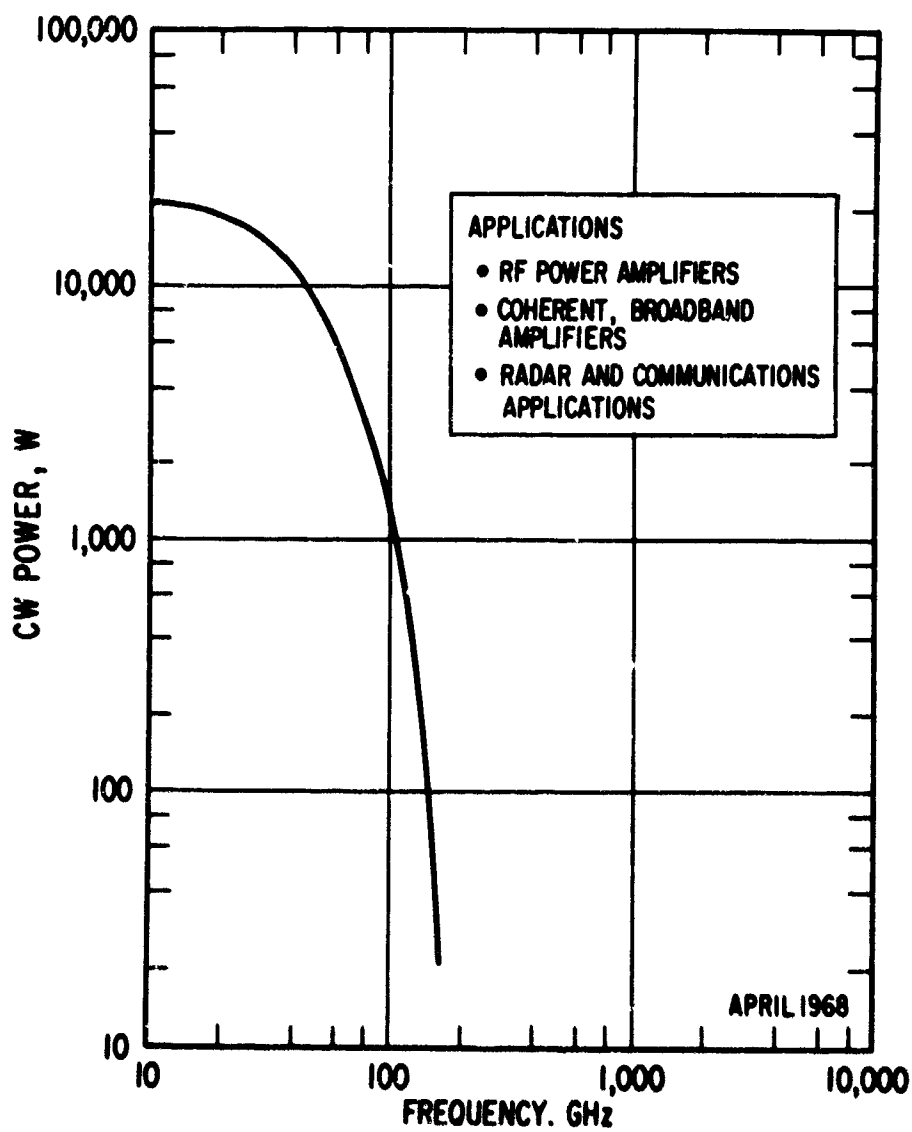


Fig. 29. Traveling-Wave-Tube Amplifiers CW Capability (State of the Art, 1970)

severe performance limitations arise because of intense electron bombardment and excessive heating. For these reasons, the terminal useful output of the conventional magnetron configuration probably occurs in the 150- to 200-GHz region. The magnetron is presently available for use in short-pulse millimeter radar systems. The peak power outputs range from 150 kW at 40 GHz to 10 kW at 94 GHz, Figure 30. To achieve high radar range-resolution goals and also to maintain low average power levels, operational millimeter-wave magnetrons characteristically employ pulse widths in the order of nanoseconds. The overall efficiencies of existing millimeter-wave magnetrons range from about 25% at 40 GHz to 9% at 94 GHz. The theoretical overall efficiency of the inverted coaxial magnetron configuration is estimated to be 12% at 94 GHz.

C. RECEIVERS

This section discusses the state of the art of millimeter wavelength receivers. For convenience, the material is divided into four parts: detectors, amplifiers, mixers, and medium-power sources. Power sources are included in this section on receivers because of their use as local oscillators and amplifier pump sources.

1. DETECTORS

A variety of detector types are available, including diode rectifiers, Golay pneumatic detectors, room-temperature bolometers, cooled bolometers (germanium and indium antimonide), and photoconductive detectors. All of these types of detectors have their own specialized area of application in the millimeter wavelength region and, in general, no direct comparison can or should be made between them. In general, the details of the system in which

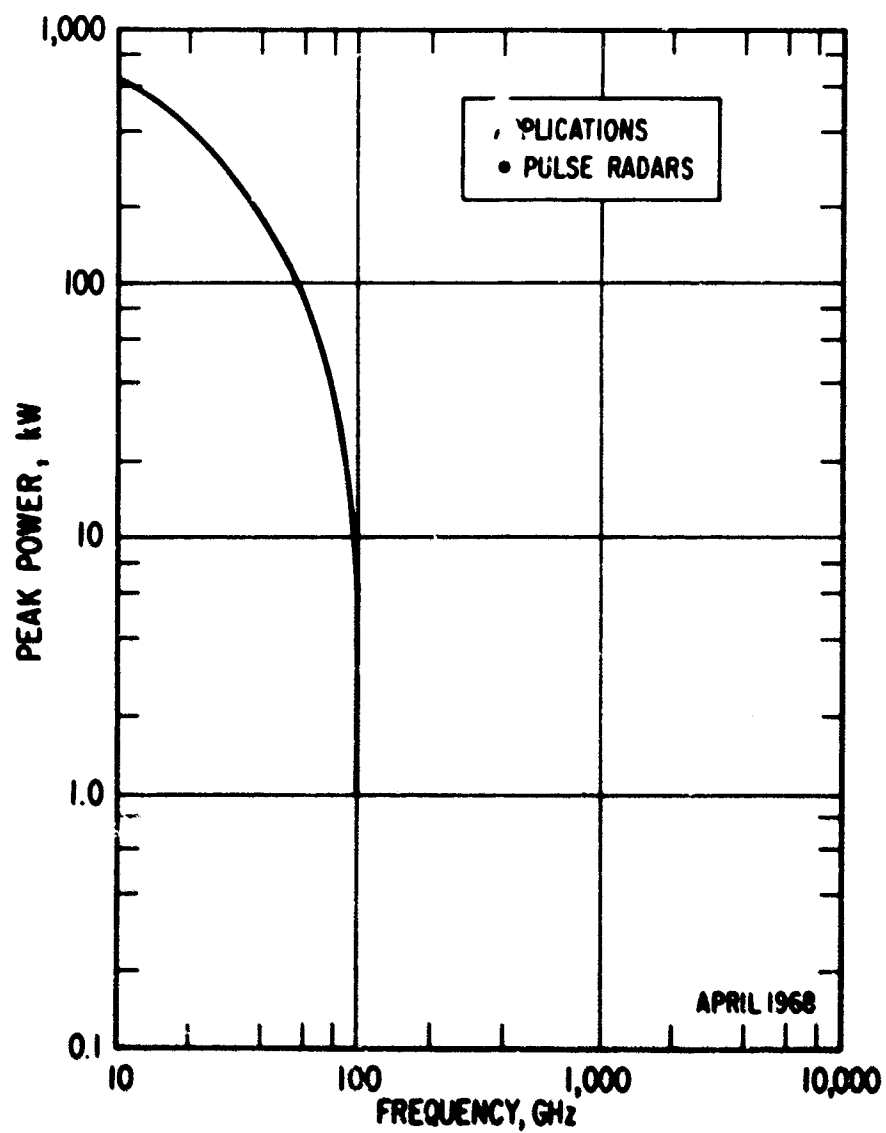


Fig. 30. Magnetrons Peak Power Capability
(Pulse Widths $< 1 \mu\text{sec}$)
(State of the Art, 1970)

the detector is to be applied must be known before a choice of detector type can be made.

Among diode-rectifier-type detectors, the silicon point-contact diode has shown the highest sensitivity for frequencies above 70 GHz. It has been used up to 300 GHz. Below 70 GHz, tunnel diode detectors show a slight advantage over the silicon point-contact diodes.

Room-temperature bolometers are useful for making relative power measurements when high sensitivity is not needed. These are used mainly in laboratory bench test where broadband operation is advantageous.

When the ultimate in detector sensitivity is required, a cooled indium antimonide bolometer can be used. These detectors are cooled to a few degrees Kelvin.

2. AMPLIFIERS

Low-noise amplifiers at frequencies greater than 70 GHz have not been built. Degenerate parametric amplifiers have been built at 35 to 70 GHz. The 35-GHz amplifier had a 3-dB noise figure (double sideband). Several major attempts have been made to show parametric action at 94 GHz, with no real success. The feasibility of amplifiers utilizing resonance saturation effects in a gas at 257 GHz has been shown, but poor noise performance and the practical problems of keeping it operating limit its usefulness. Masers have been developed up through the 35-GHz frequency range with low-noise temperatures, and amplification has been shown at frequencies up to 90 GHz, but no noise figure data are available. TWT amplifiers have been built up to 94 GHz, but the noise figure was greater than 15 dB at 94 GHz.

3. MIXERS

Fundamental mixing has been utilized up to 220 GHz. However, for frequencies over 100 GHz, harmonic mixers are more popular since suitable local oscillator sources are not readily available. A harmonic mixer is one in which a harmonic of the local oscillator mixes with the incoming signal to produce a difference signal. Figure 31 shows some of the conversion loss measurements for fundamental and harmonic mixers. The point contact diodes are too fragile for system use other than laboratory-type environments. GaAs diodes have shown the lowest conversion loss at 94 GHz, less than 6 dB. Although Schottky barrier diodes have been demonstrated in the laboratory to 94 GHz, there are none available commercially with low conversion loss above 50 GHz. However, it is expected that they will be available to 100 GHz by the end of 1968. The evaporated contact and passivated surface of the Schottky barrier diodes permit mixers with good mechanical as well as electrical characteristics. They are reproducible and less subject to burnout than the point contact diodes. Upconverters using varactor diodes have been constructed at 50 GHz with performance as good as an equivalent microwave device. There are varactors that just now are coming on the market, however, that will permit this type of device to be developed up to 100 GHz.

4. MEDIUM POWER SOURCES

Klystrons have been built for frequencies to 220 GHz with milliwatts of output power. However, performance and life have been poor above about 70 GHz. For applications where klystrons are not particularly suited, varactor multiplier chains have been developed. Complete solid-state multiplier chains have been built to 94 GHz with 12 mW of output power and 220 GHz with 3 mW.

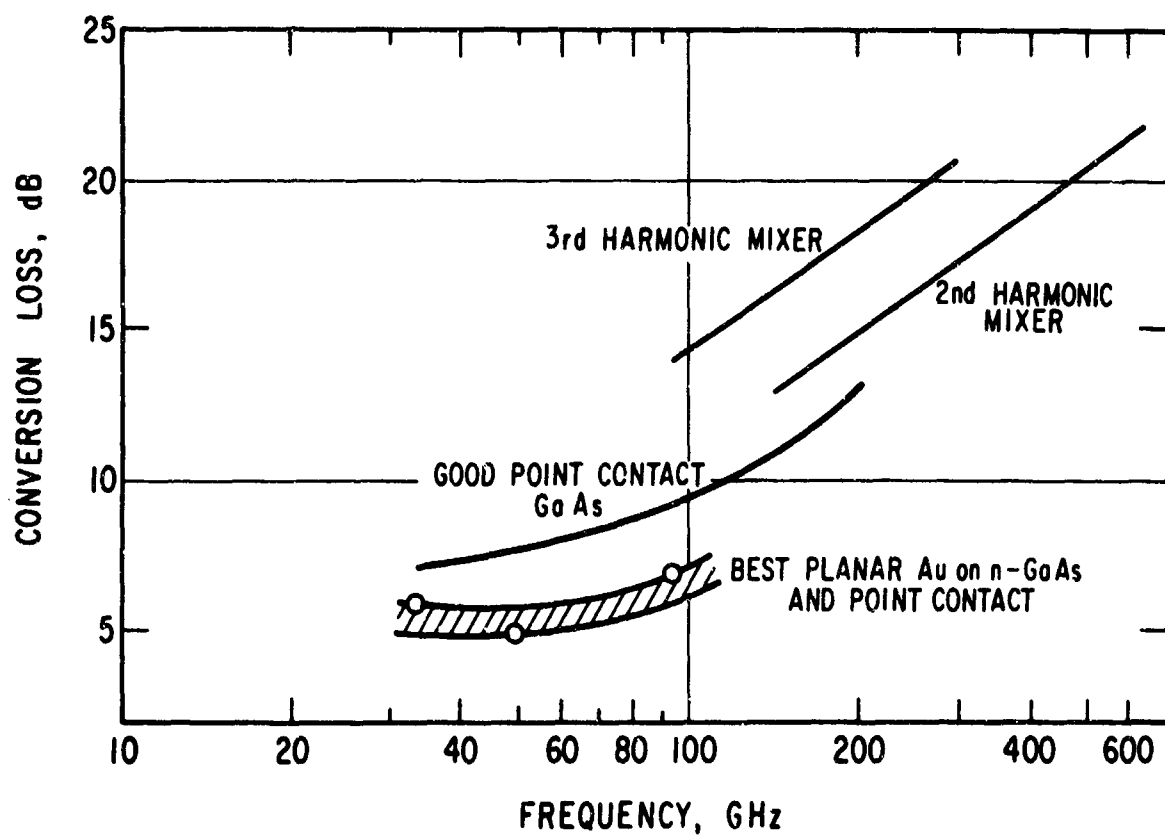


Fig. 31. Conversion Loss of Typical Mixers

Resistive multipliers have provided detectable harmonic power output to greater than 600 GHz, but the power output varies inversely with the square of the harmonic number. Varactor multipliers have been constructed yielding 20 mW at 140 GHz in a doubler circuit with 20% efficiency. Conventional packaged varactor diodes have been used effectively to 50 GHz for output powers of several hundred milliwatts, but packaged diodes have not been effectively applied at higher frequencies. Varactor multipliers are limited to relatively low-power operation by fundamental device parameters that restrict the physical size of the device. This restriction is related to the fact that the transit time of carriers across the active region must be a small fraction of a wavelength.

In 1958, Read of Bell Telephone Laboratories proposed a device in which the transit time of the carriers was a large part of the period. In 1963, J. B. Gunn observed the "Gunn" effect, and it, too, utilized a carrier transit time equal to the period of the operating frequency. Figure 32 shows the geometry of the various bulk-effect oscillators that show great promise for future use in the millimeter-wavelength portion of the spectrum. Figure 33 is a plot of power performance vs frequency for various solid-state sources. The power varies approximately as f^{-2} . Using this frequency dependence to extrapolate the better performance numbers gives a good indication of the potential across the whole millimeter wavelength range for an equivalent technology development. The efficiency of the Gunn oscillator is typically 5% (with 26% reported) and typically 7% for Impatt (impact avalanche transit time) diode oscillators. An anomalous avalanche oscillator with a 60% efficiency has been reported. These

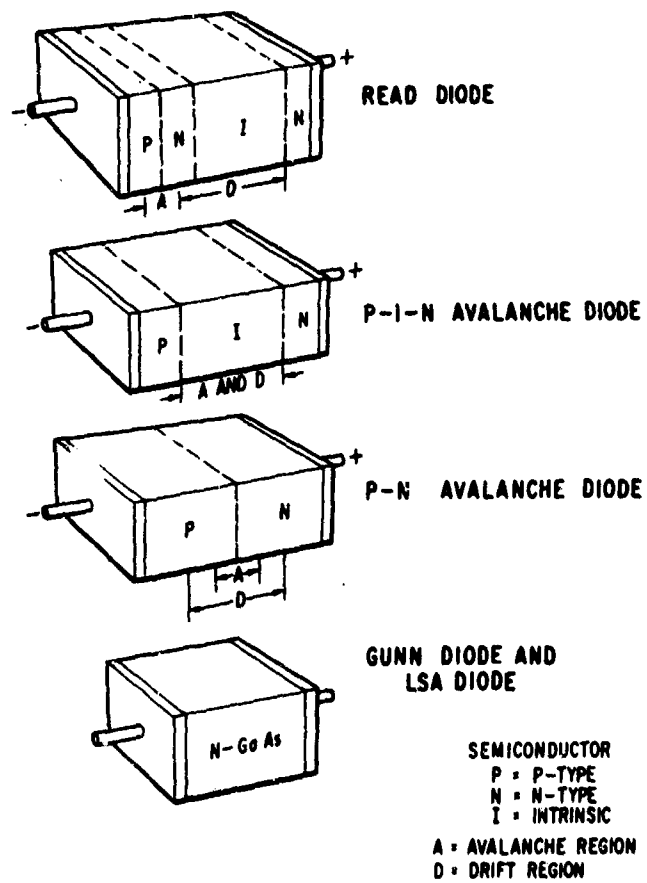


Fig. 32. Geometry of Various Bulk-Effect Oscillators

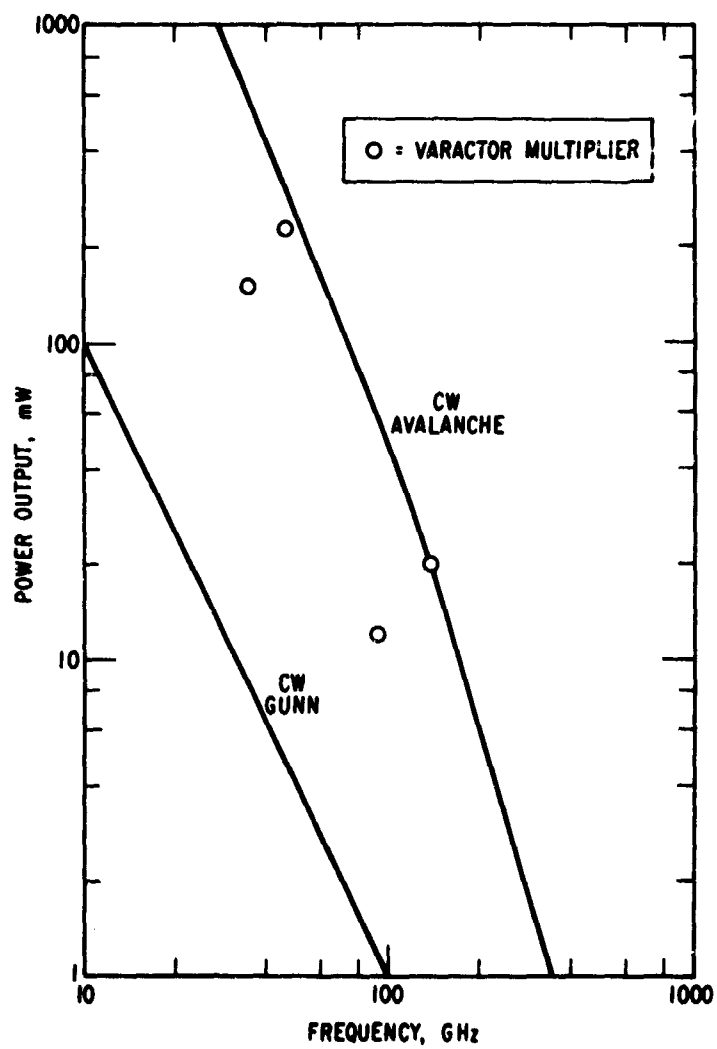


Fig. 33. Power Output vs Frequency of Solid-State Sources

new oscillators are voltage tunable and can be injection locked to a stable lower-power source. These oscillators may be operated in parallel, in series, or in parallel-series for more power output. The parallel-series combinations allow impedance matching. Figure 33 is based on a collection of laboratory results and may represent power densities approaching device burnout. Optimum circuit development for these devices has not been achieved, and much effort is being expended in increasing power and reliability.

The future efforts on bulk-effect oscillators should produce, by 1970, reliable devices in well-developed circuits suitable for millimeter-wavelength systems. The Schottky barrier diode mixers should also be well developed, and it is expected that they would be commercially available. Parametric amplifiers with solid-state pumps suitable for experimental systems are forecast for 1970.

The 1970 millimeter-wavelength space systems should have less than a 10-dB noise figure; the 1970 ground systems should have less than an 8-dB noise figure, with a receiver reliability not previously available at millimeter wavelengths.

IV. HIGH-RESOLUTION RADAR

Theoretical studies at The Aerospace Corporation of the general radar resolution problem have been the stimulus for the initiation of an experimental program aimed at demonstrating that the theoretical resolution potential inherent in millimeter-wave radar is, indeed, practicable.

At EHF, as is well known, the available bandwidth is extremely large. Also, component availability is no longer a major limiting problem in implementing experimental systems, as attested to by several years of The Aerospace Corporation laboratory fabrication and test and by the recent delivery of a 94-GHz TWTA, which included specifications for millisecond pulse durations at peak power outputs approaching 1 kW. In addition, the experience and knowledge gained in the implementation of millimeter-wave equipment for, and in the making of, measurements of atmospheric attenuation, absorption, and dispersion [13, 14] have been important factors in the decision to implement a radar at millimeter waves to test high-resolution principles. The eventual goal of this project is the demonstration of the feasibility of obtaining radar echoes from various orbiting objects that will be suitable for processing so as to obtain a detailed image of the satellite.

A. APPROACH

The approach to the eventual goal of a millimeter-wave satellite identification radar has been that of a series of experiments designed to determine the performance limitations of the components involved, followed by experimental measurements on the integrated radar system. The radar is planned around two millimeter-wave tubes, a 3-W BWO, and a 1-kW TWTA.

The driver, a Hughes Research Laboratories BWO Type LOW-1, has been under evaluation at The Aerospace Corporation for several months.

In the planned experiments, the 3-W BWO will be frequency-modulated linearly over a bandwidth of 1 GHz with pulse widths of up to 1 ms in duration at 10% duty ratios. Long-pulse operation is required at these power-limited frequencies to provide sufficient energy "on target" so that a usable system S/N may be obtained. The 10% duty ratio is the specification limitation on the final TWTAs, the 1-kW Hughes Research Lab HAW-3, which was designed specifically for long-pulse operation.

The 1-kW TWTAs have been integrated with the 3-W BWO, and radar echoes over a 10-n mi test range have been obtained. Preliminary evaluation of the resolution capabilities of the system will be done by the use of range and azimuth spaced targets at this 10-n mi distance. It is felt that satisfactory completion of the above experiments will yield the necessary experience and know-how to ease the problems anticipated in obtaining satellite echoes.

These latter system configurations would all include combining the LOW-1/HAW-3 linear FM pulsed ("Chirp") radar with the Aerospace precision millimeter-wave 15-ft-diam (4.57-m) dish for satellite echo experiments. Maximum pulse lengths of 1 ms can be utilized in these configurations in obtaining echoes at distances greater than 100 n mi. Expected S/N exceeds 10 dB.

For the satellite echo tests, the 15-ft dish would be programmed to follow a chosen space object by means of "stored" ephemeris data fed into the digital computer that is employed for the antenna pointing and control

requirements. The practicability of tracking space objects in this manner has been tested satisfactorily on such satellites as Echo and Pegasus, wherein pointing confirmation was obtained by use of optical tracking techniques.

Preliminary experiments have included a very short-range indoor test with FM of the LOW-1 followed by similar tests, though more complex in scope, over outdoor test ranges to 10 n mi and have included the 1-kW TWTA. These tests were necessary for familiarization with tube and circuit behavior and to show feasibility of the modulation techniques planned for the more complex experiments to follow. The results of these preliminary experiments are discussed in the next section.

B. EXPERIMENTAL RESULTS

An eventual system configuration envisioned for obtaining satellite echoes is shown in simplified block diagram form in Figure 34. After an FM echo pulse is received, an identical FM pulse will be generated at some small time offset so that, for linear FM pulses, the difference frequency output from the mixer is a constant frequency within the pulse period for a fixed target. The effects of Doppler, beyond a mere translation of the signal spectrum, are discussed in detail in a companion paper [15].

The very difficult problem of processing extremely large time-bandwidth products has led to the choice of the linear FM pulse as a means of making this processing practical. Repeatability of this sweep is mandatory in the system envisioned, since there are no means by which the transmitted signal can be delayed so that the delayed version can be used in the correlator. Thus, the repeatability requirement is independent of whether the sweep is linear or nonlinear.

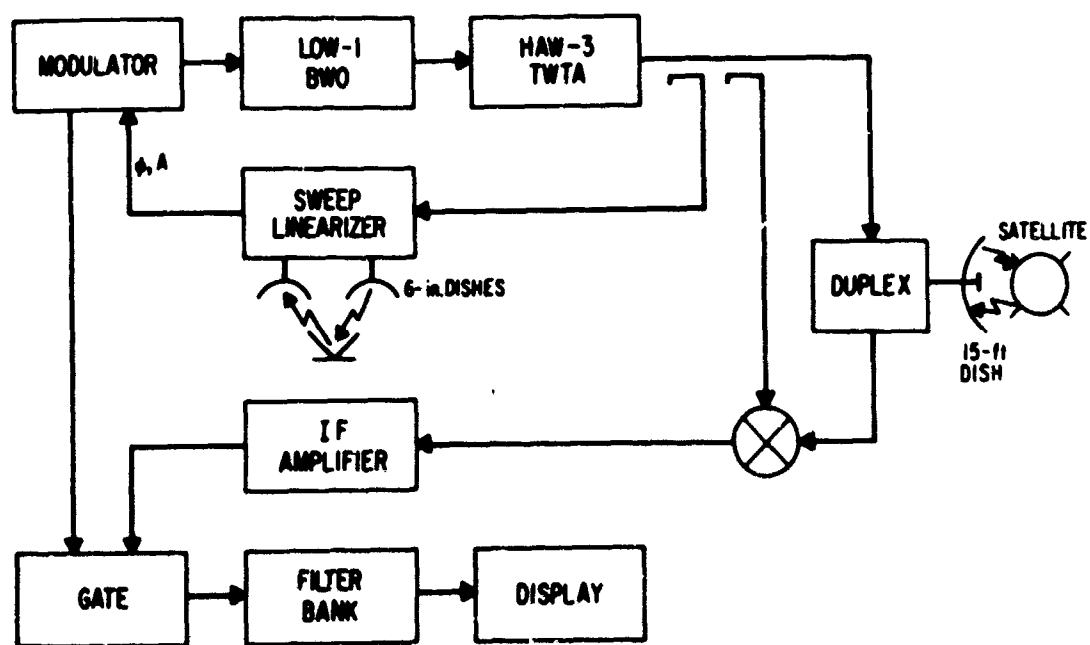


Fig. 34. Millimeter-Wave Radar Configuration

The requirements on linearity of the FM pulse are dictated by the processor. Only if the sweep is linear will targets from a different range (or individual scatterers of a satellite) be properly correlated so that range can be determined from finding the center frequency of the mixer output. If it were necessary to meet this requirement for the total radar-range capability, then an extremely high degree of linearity would be mandatory for the entire sweep. However, because the satellite position will be known, it is necessary to investigate only a small range interval about its position (its range spread), and thus the system contemplated now becomes practicable. The reference sweep can be centered on the range interval of interest at a minimum time difference with respect to the received signal such that the frequency spread of the correlated output is minimized when these signals contain departures from linearity.

The remaining linearization requirement, however, is still not easily accomplished. Considering the extremely large time-bandwidth products involved and the existing state of the art in millimeter-wave components, nonlinearities in the frequency sweep will inevitably occur due to imperfections of these components. Thus, it is of considerable importance to determine the extent of these nonlinearities and to develop techniques for their minimization, as well as to ensure the repeatability of the waveform. An estimate of the required linearity is derived in Appendix A.

The 3-W BWO has been operated in the laboratory, and its static parameters have been measured. Its dynamic characteristics are being studied in a radar test setup. Several ranges have been operated to date. The first

range was in the laboratory with a one-way distance of 20 ft (6.1 m), where a planar mirror target was used. The others included outside ranges with one-way distances of 390 ft (119 m) and 600 ft, where a corner reflector was used. In all cases, swept FM was employed, with capabilities of sweeping in excess of 1 GHz in 1 ms. The radar setup (Figure 35) consists of two 6-in. (15-cm) antennas with a coupler-mixer arrangement such that the RF return signal can be heterodyned with a portion of the transmitted signal. The difference beat signal thus produced is determined by the round-trip delay time τ and the ramp rate of the swept RF signal [$f = (df/dt)\tau$]. For the indoor laboratory range, τ was 40 ns, which, with a ramp rate of 1 GHz/ms, produced an average beat frequency of 40 kHz. The RF ramp produced by the 3-W LOW-1 is not exactly linear, however; consequently, the beat frequency varies about some average value. This variation was measured, and an indication was provided of the RF sweep nonlinearity of the LOW-1 when driven with a linear ramp control function.

The shorter outside range provided a τ of approximately 0.8 μ s, and with an RF sweep ramp of 1 GHz/ms, produced an average beat frequency of 800 kHz. As a means to study the deviation characteristics of the beat signal, an FM discriminator was constructed and incorporated into an FM feedback loop. Figure 36 is a plot (top curve) of the open-loop beat-frequency deviations derived from the 390-ft test range by use of the 1-GHz/ms sweep. The RF sweep covered the range from 94 to 95 GHz. The maximum peak-to-peak deviation of the beat frequency was approximately 850 kHz with a maximum rate of deviation approximating 34 kHz/ μ s.

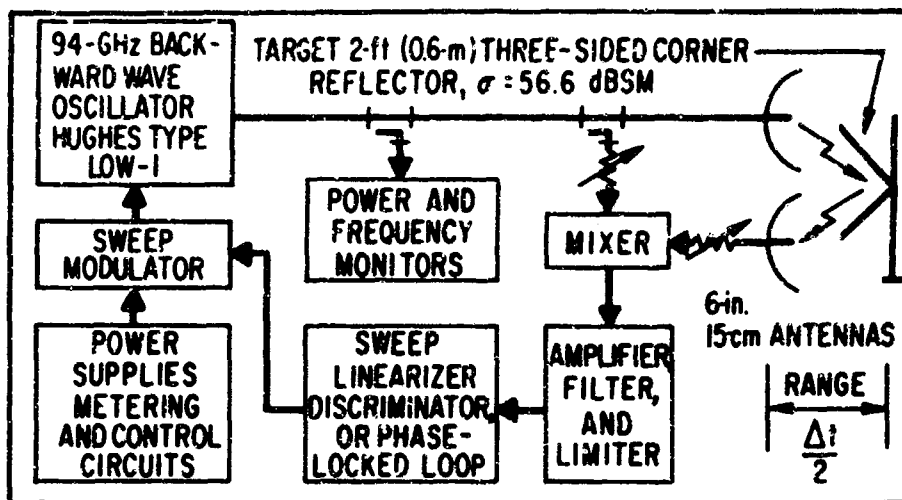


Fig. 35. Short-Range Millimeter-Wave Radar Test Setup

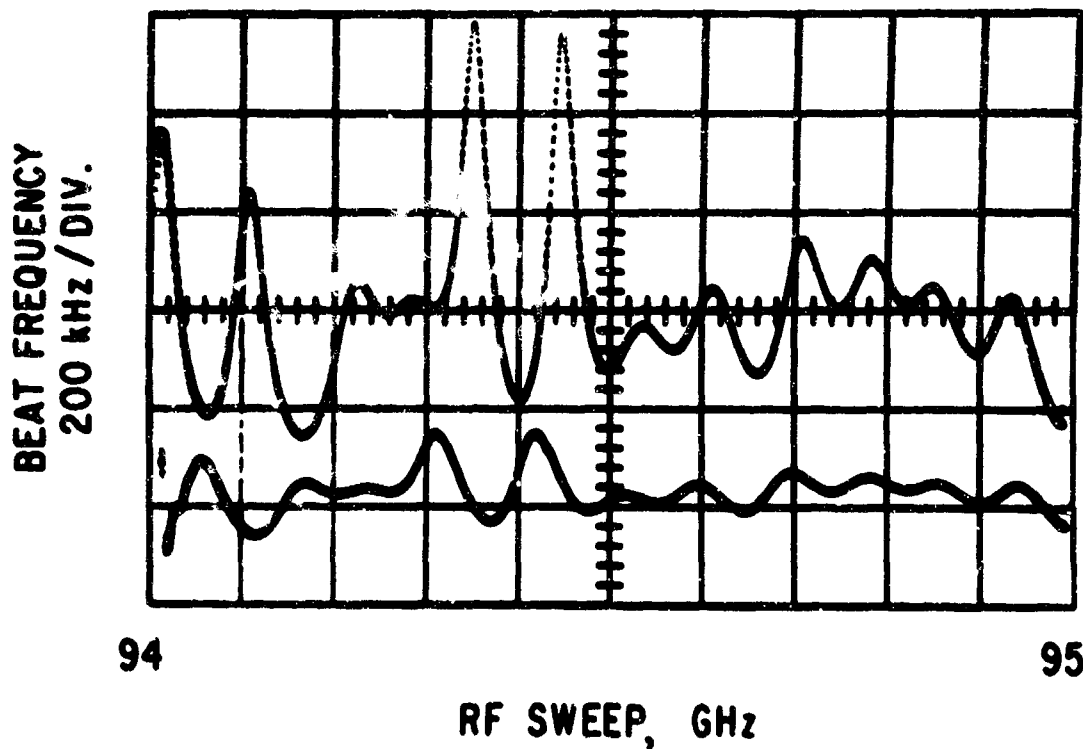


Fig. 36. Comparison of Open-Loop (Top) and Closed-Loop (Bottom) Beat-Frequency Deviations; FM Feedback Loop.
Low-I, $T = 1$ msec, $\tau = 0.8$ μ sec

Figure 36 also indicates (bottom curve) the improvement obtained by the FM feedback loop in reducing the beat-frequency deviations caused by nonlinearities in the transmitted frequency ramp; these nonlinearities were reduced by about a factor of 4 and the maximum rate of deviation was less by a factor of 6. The primary cause of these nonlinearities is thought to be frequency-dependent mismatches between the slow-wave structure and the output coupling section of the BWO.

Because of the high rate of change of the beat-frequency nonlinearities, the relatively long range delay parameter, and the base bandwidth limitation of the discriminator, it was not possible to employ sufficient loop gain in the FM feedback loop to linearize the RF sweep to the degree desired before the loop became unstable. A phase-locked feedback loop was therefore developed to provide the desired degree of RF sweep linearization.

A block diagram of the system for phase-lock linearization of the FM sweep is shown in Figure 37. All components are the same as those used in the FM feedback system, except the phase detector, filter amplifier, and reference oscillator. The phase-lock loop must have high gain and wide bandwidth for tracking the nonlinearities in the 3-W LOW-1. In this system, the maximum loop bandwidth that can be achieved with stability is limited by the time delay and phase shift around the loop. The loop will tend to oscillate at a frequency where the phase shift, including that due to the time delay, is approximately 90 deg.

The loop delay consists of the propagation delay and the delay of the sample and hold-phase detector. The phase-detector delay is one-half of the

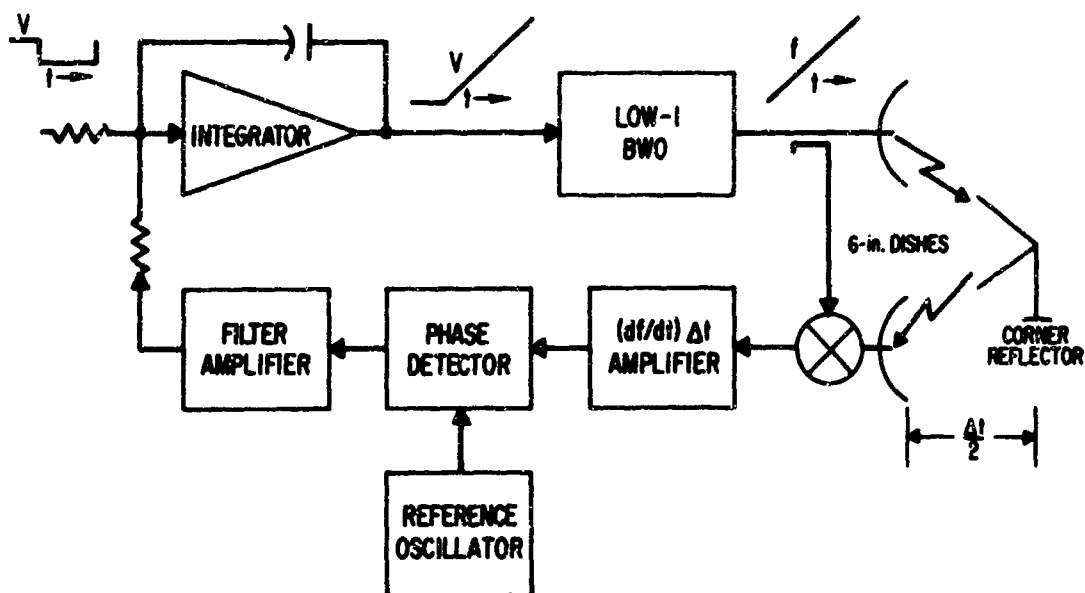


Fig. 37. Phase-Lock Sweep Linearization

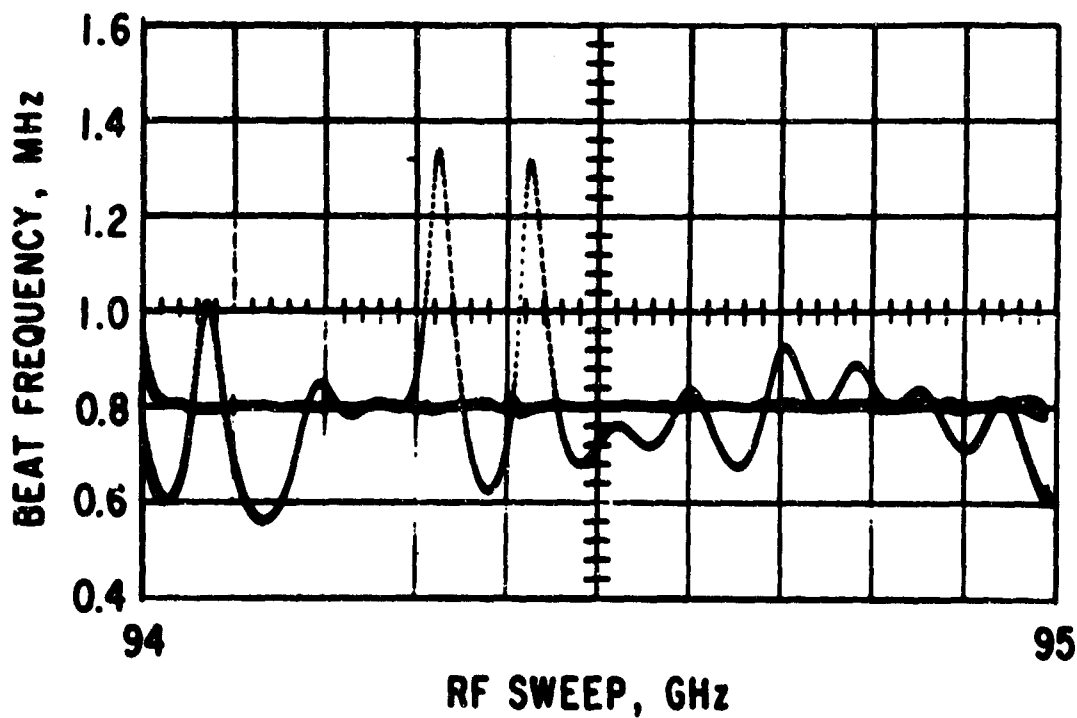


Fig. 38. Comparison of Open-Loop and Closed-Loop Beat-Frequency Deviations; Phase-Locked Loop Low- Q , $T = 1$ msec, $\tau = 0.8$ μ sec

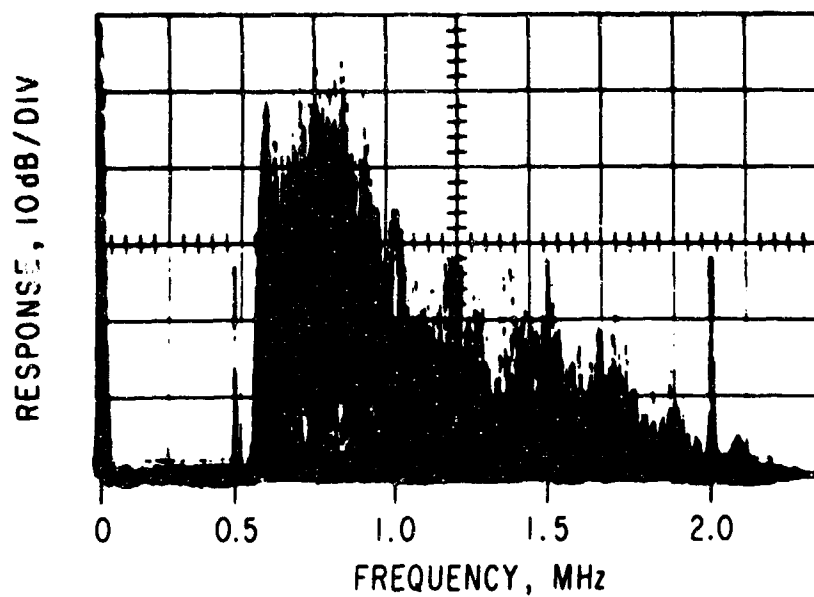


Fig. 39(a). Beat-Frequency Spectrum
Open Loop

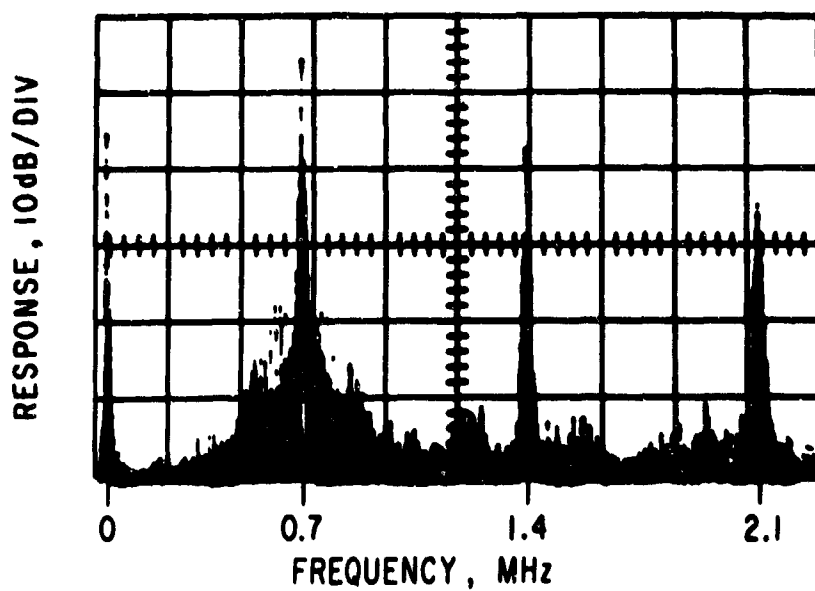


Fig. 39(b). Beat-Frequency Spectrum
Phase-Locked Loop

storage time. Thus, for a given frequency ramp rate, there is an optimum propagation delay time that gives minimum loop delay (see Appendix B). At the planned sweep rate of 1000 MHz/ms and with a two-sample-per-cycle phase detector, the minimum loop delay occurs when the propagation delay and the phase detector are each 0.5 μ s. The maximum loop bandwidth should approach 250 kHz. With a four-sample-per-cycle phase detector, the optimum propagation delay and phase detector delay is 0.353 μ s and the maximum loop bandwidth is 353 kHz. Because of filtering and phase shift problems, it has been necessary to operate the linearization loop with propagation delays somewhat longer than the theoretical optimum. Efforts are being made to reduce the delay and to increase the loop bandwidth and gain. Through this effort, a further improvement in FM sweep linearity should be achieved.

Figure 38 indicates the improvement obtained by the phase-locked loop in reducing the beat-frequency deviations caused by the nonlinearities in the transmitted frequency ramp; these beat deviations were reduced to less than 20 kHz, peak to peak. The propagation delay was 0.8 μ s, as before, with a ramp rate of 1 MHz/ μ s.

The spectrum of the frequencies generated in the open-loop mode over the 390-ft range is shown in Figure 39(a). Maximum energy is indicated at about 700 kHz, with significant components to 2 MHz. The passband of the radar mixer preamplifier is slightly greater than 2 MHz. The spectrum in the closed-loop mode is shown in Figure 39(b). The 700-kHz beat frequency can be clearly seen with a S/N of 40 dB. The spectrum in the ideal case of a perfectly linear RF sweep would be a single spectral line with $\sin x/x$

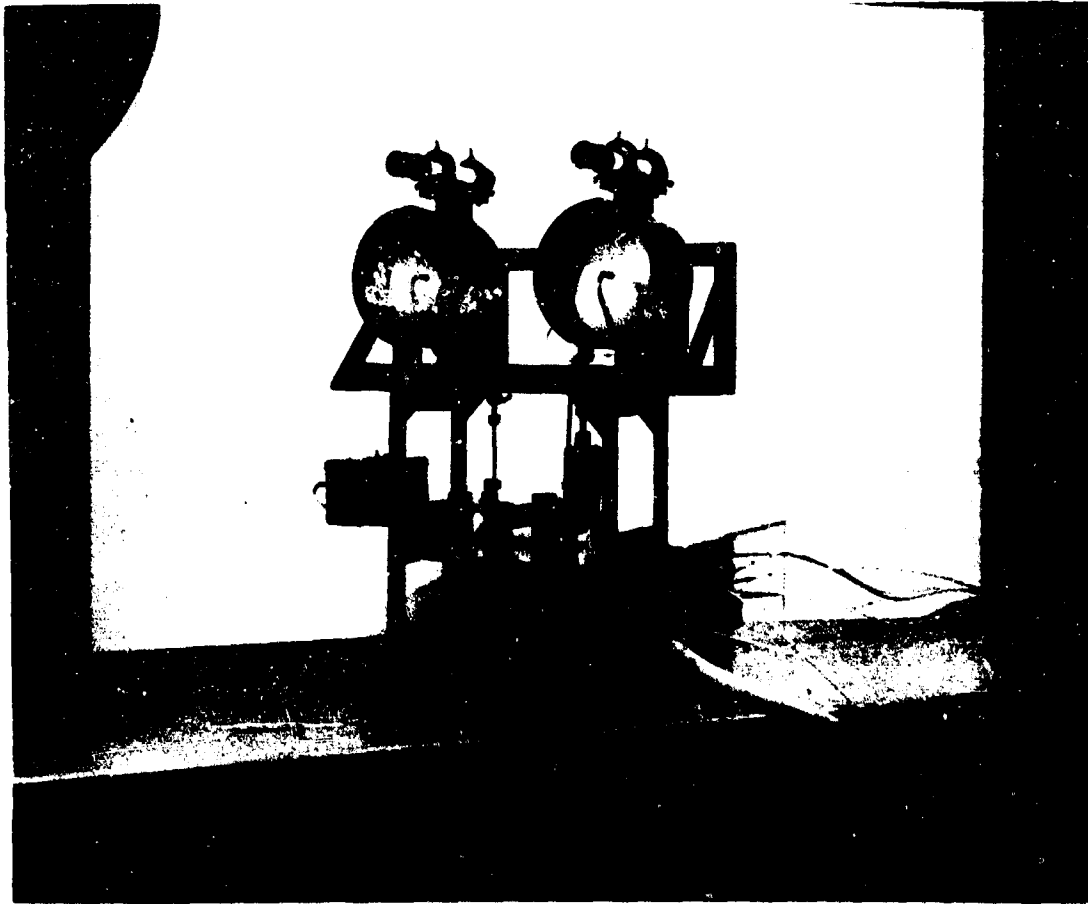


Fig. 40. Radar Equipment (Short-Range Test Setup)

components due to the pulse rate. Harmonics of the beat frequency, residual noise, and $\sin x/x$ components are also evident because of the broad bandwidth of the mixer preamplifier.

This accomplishment represents a significant achievement and is a necessary first step toward the eventual goal of the planned long-range radar. The short-range auxiliary radar will be used in conjunction with the high-power long-range radar as a sweep linearizer as shown in Figure 34.

A photograph of the transmitting and receiving antennas, waveguide components, and the BWO of the radar test setup appears in Figure 40.

C. CRITICAL CONSIDERATIONS AND CONCLUSIONS

Major critical components required for the millimeter-wave radar, in addition to the power tubes and linearizer discussed previously, include a low-loss transmission line, mixers, and a duplexer. These components have been a part of laboratory investigations, and progress has been achieved in these development efforts.

Many millimeter diode mixers were evaluated during the past year. The laboratory developments mainly concerned gallium-arsenide diode life-time problems. A promising combination of doping level ($> 2 \times 10^{18}$ carriers/cm³) of the gallium-arsenide semiconductor and a gold alloy whisker material was developed. These diodes have given excellent electrical performance and good lifetimes without requiring a hermetically sealed package. The conversion loss at 94 GHz is less than 6.5 dB. These developmental diodes gave better than a two-to-one improvement (over other available diodes) in system sensitivity for the existing 94-GHz radiometric facility with an IF bandwidth of 2 GHz (2 to

4 GHz). A balanced mixer with a low IF, developed for the initial testing on the radar program, has been completed and is being employed in the experimental system. (Figure 41).

The development of a 94-GHz, 1-kW duplexer was initiated in the laboratory since none was available from industry. An electromechanical TR (transmit-receive) switch was fabricated to meet these requirements. Figure 42 shows the basic construction of this device. During the transmit period, the waveguide is made to look like a section of waveguide beyond cutoff, resulting in an effective short with low leakage through the TR switch. In the receive period, a thin metal ridge is introduced into the waveguide. The ridge lowers the cutoff frequency, allowing signals above this frequency to propagate through the waveguide. An experimental model of the TR switch had an insertion loss of 1 dB in the receive mode and an isolation greater than 50 dB in the transmit mode; switching time was approximately 100 μ s.

Another major problem under investigation is the mounting of the 1-kW HAW-3 in conjunction with the 15-ft dish so as to minimize the transmitting losses. For 94-GHz operation, the conventional rectangular waveguide exhibits a 0.5-dB loss/ft since placing the radar on the antenna structure is undesirable because of weight restrictions (other equipment is placed on the antenna, which is in constant use for other research activities); a low-loss system of oversize waveguides and quasi-optical waveguide transmission lines (beam-waveguide) is being designed so that both the radar receiver and transmitter can be placed at the bottom of the antenna tower. Such a waveguide system is expected to yield an approximately 4-dB two-way attenuation. The

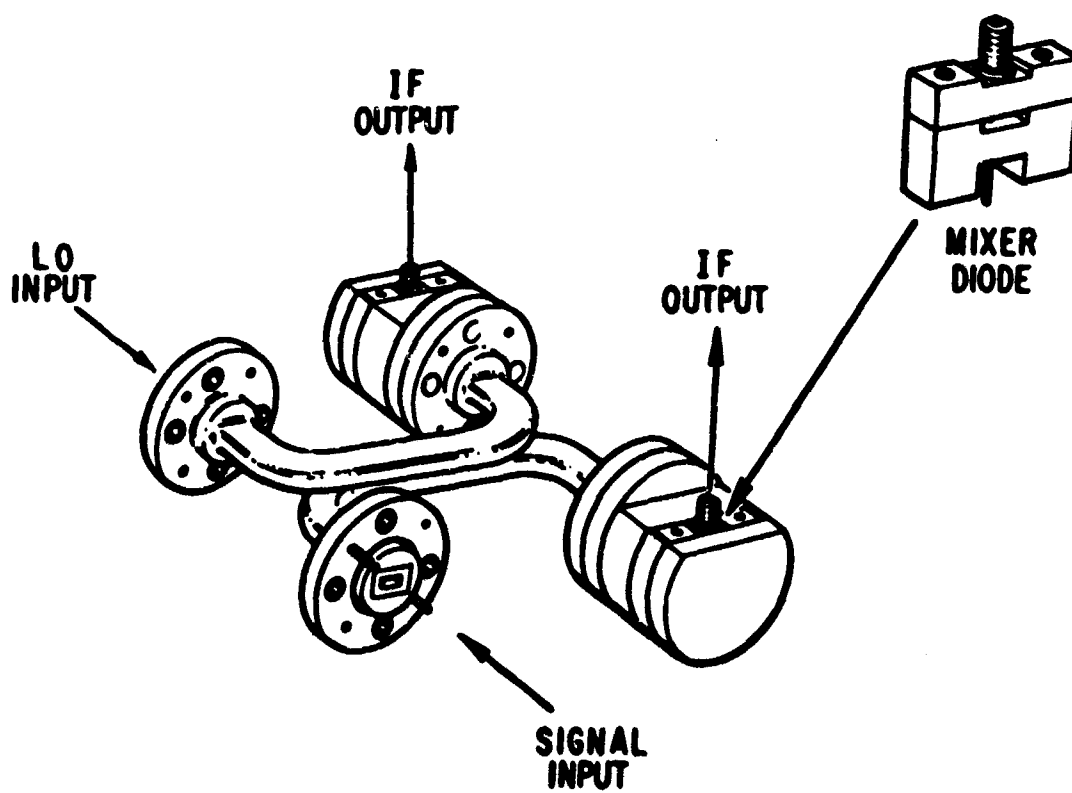


Fig. 41. Mixer Unit

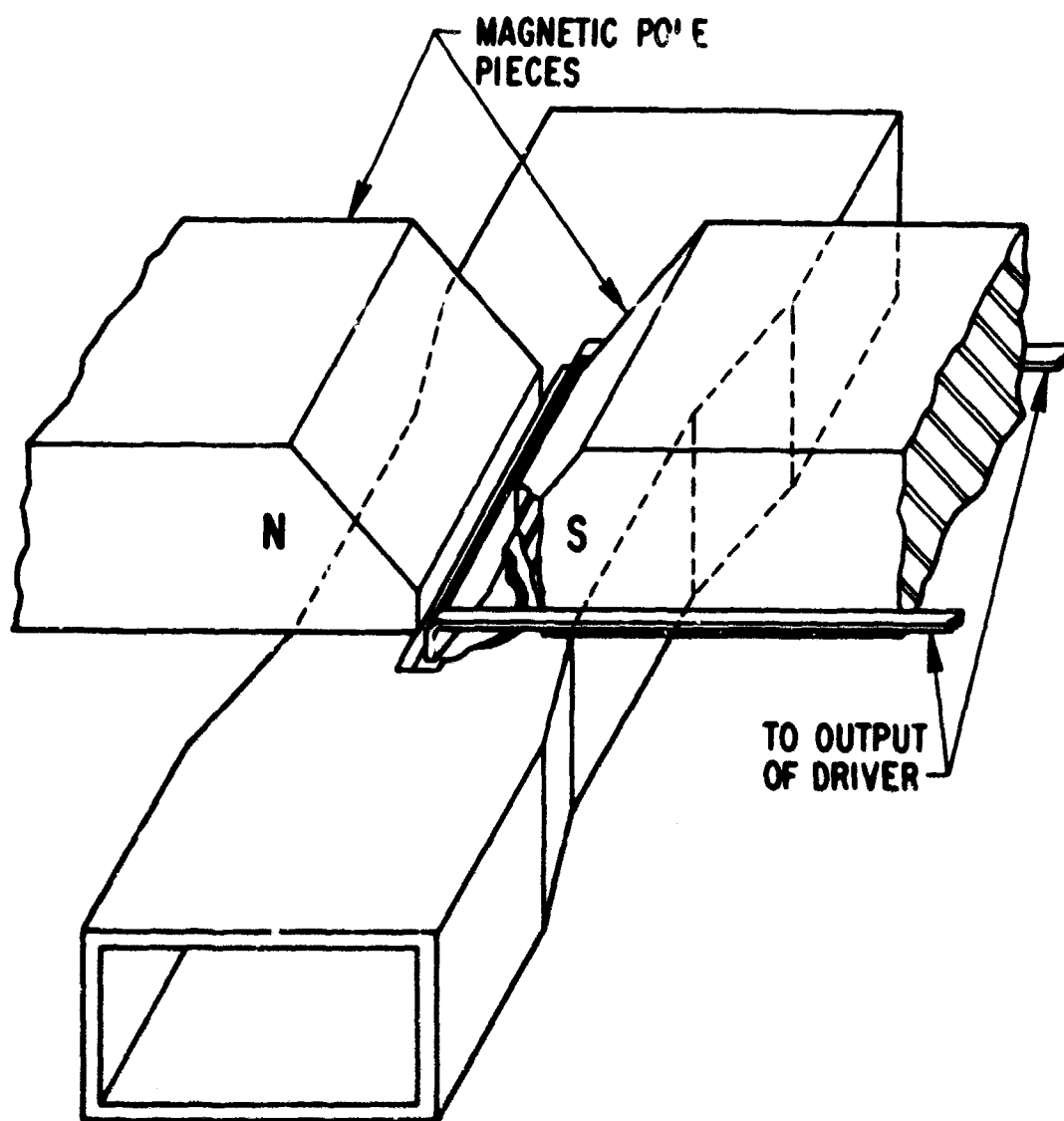


Fig. 42. Electromechanical TR Switch

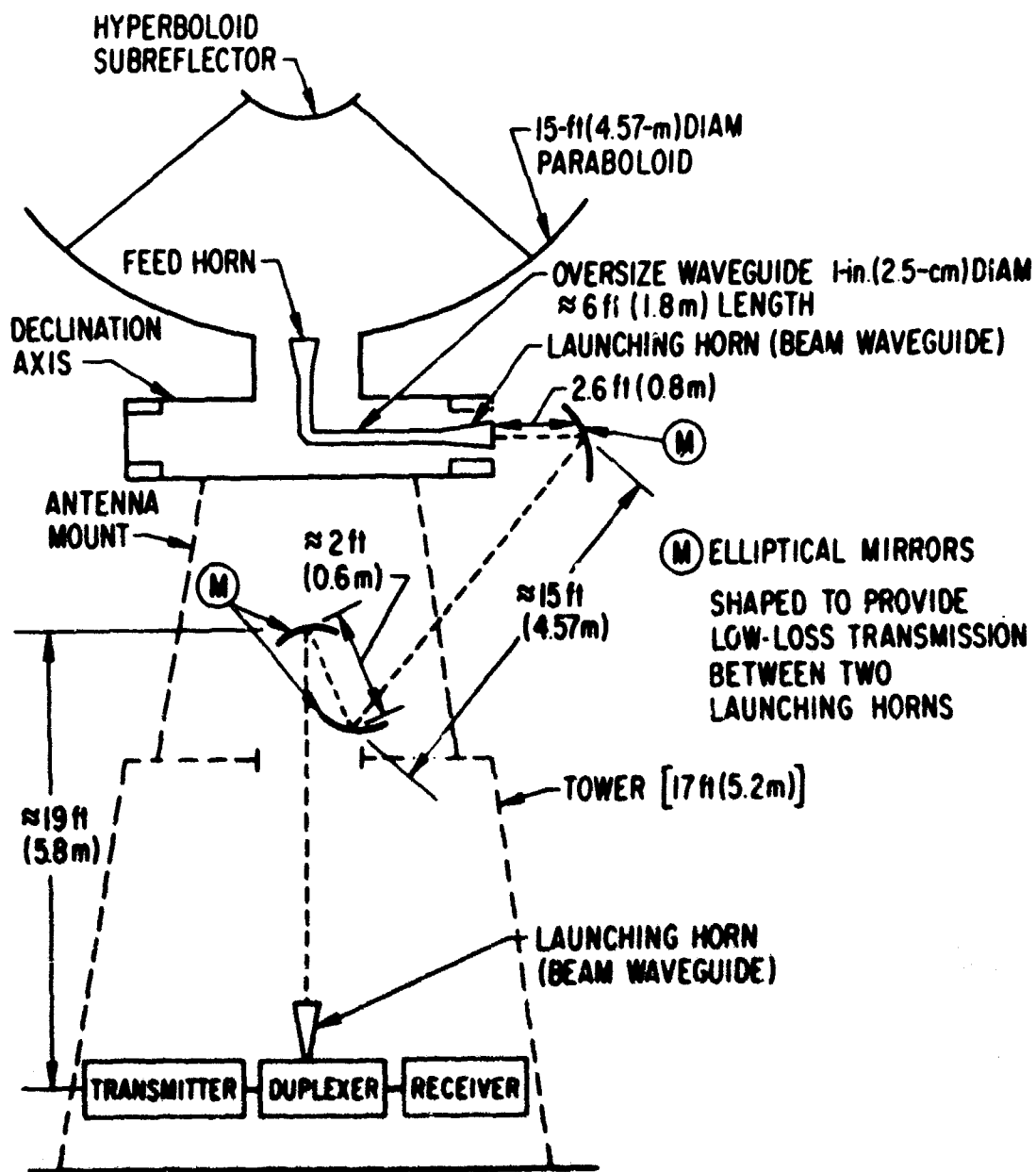


Fig. 43. Beam-Waveguide System

tremendous mechanical advantages and the simplified logistics of placing the radar electronics on the "ground" floor make the development of a low-loss transmission system extremely advantageous. Of perhaps greater importance is the ease with which adjustments and observations of experimental changes may be made with the equipment in a laboratory-type environment. An operational system would probably be configured with the transmitter and receiver preamplifier on the dish, wherein the 4-dB two-way loss could be reduced to below 2 dB.

The feasibility of the beam-waveguide concept was demonstrated by the use of two paraboloidal reflectors, in lieu of an ellipsoidal reflector, in a crude laboratory setup. Tests indicated that it was possible to lengthen a 10-in. (25-cm) transmission line to 40 in. (1 m) without additional insertion loss. With the feasibility demonstrated, the design of the shaped mirrors is now under way. Figure 43 is a two-dimensional sketch showing pertinent details of the proposed beam-waveguide system in conjunction with the 15-ft antenna.

Feasibility has been demonstrated in all major critical areas of a large time-bandwidth product millimeter-wave radar. It remains to determine the limitations on high-resolution radar of practicable systems.

V. SATELLITE-TO-SATELLITE COMMUNICATIONS

A. EARLY SATELLITES

The use of satellites in communications systems has spanned but a few years, yet the variety and diversity of these systems is already quite extensive. The use of satellites for communications relay between widely separated earth locations was a subject of wide discussion that preceded our earliest satellites.

Historically, although receiving little note, the first real demonstration of a satellite communicating information between ground stations occurred on 11 October 1958. This was the unsuccessful Pioneer 1 moon probe^{*} that retransmitted the tracking and command signals sent from Cape Canaveral; these signals were received by the Jodrell Bank Tracking Station in England. The first communication experiments by satellite were also initiated in 1958 with Score, an Atlas ICBM that was orbited (less its two booster engines) with a 150-lb communication package. This satellite relayed messages between ground stations in Arizona, Georgia, and Texas for 13 days.^{**}

In July 1962, the highly successful Bell Telephone Laboratories' communications satellite Telstar was launched, and it conducted a variety of communications tests, including TV, between U.S., British, and French ground stations. Telstar was then followed by increasingly sophisticated communications satellites, such as Relay and Syncom.

^{*}In NASA's first launch, Pioneer 1 failed to reach its lunar target but did attain an altitude of 70,717 m to become the first deep-space probe.

^{**}TRW Space Log, vol. 7, No. 3.

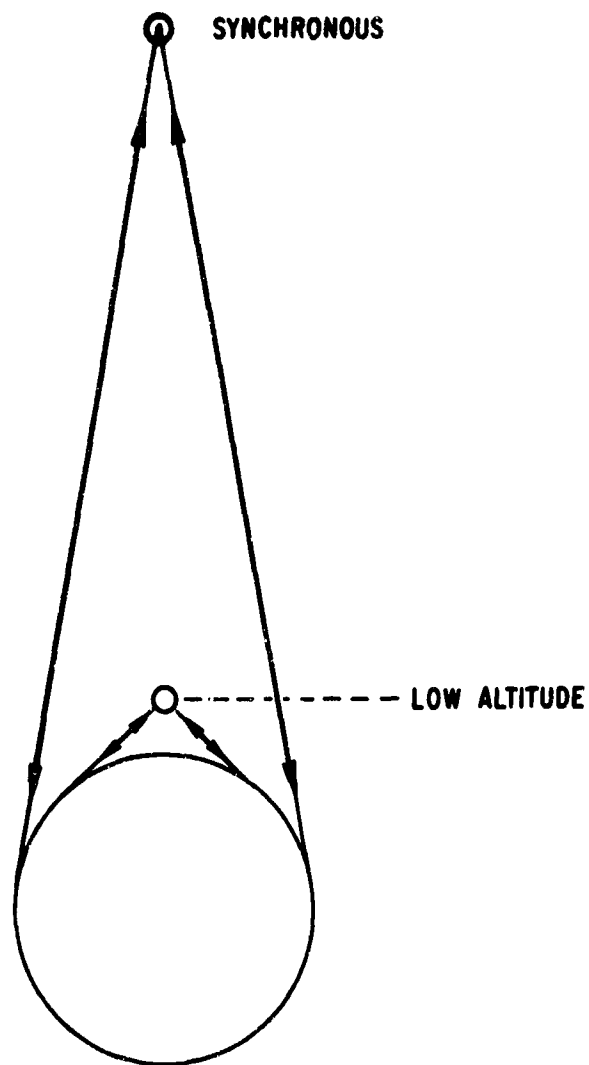


Fig. 44. Mutual Visibility for Low-Altitude and Synchronous-Altitude Satellites

B. SATELLITE CONFIGURATIONS

All of the satellites discussed, including the most recent synchronous satellites, had one common limitation: the "mutual visibility" of the relay satellite from ground terminals. Figure 44 shows the area of mutual visibility for low-altitude and synchronous-altitude satellites. Figure 45 indicates the relationship between satellite altitude and the distance between ground terminals wherein mutual visibility exists.

It is apparent that the lower the altitude of the relay satellite, the smaller is the distance between ground terminals that can simultaneously "see" the satellite. In addition, for a given distance, the time duration of visibility is a function of satellite altitude; the time duration increasing with satellite altitude.

There is no time-duration limitation for a relay satellite at synchronous orbit if the ground terminals are restricted to maximum distances that include accommodations for satellite inclination and ellipticity. The maximum distance wherein visibility exists is approximately 9750 n mi. This distance limitation can be removed by using a satellite-to-satellite relay — the primary subject of discussion in this section.

An example of a satellite-to-satellite space relay system that provides nearly global coverage is shown in Figure 46. This figure is a projection of the orbit in the equatorial plane, viewed from the pole, and indicates the geometric relationships of a three-satellite relay system. This is the minimum satellite system configuration that eliminates the distance- and viewing-time limitations.

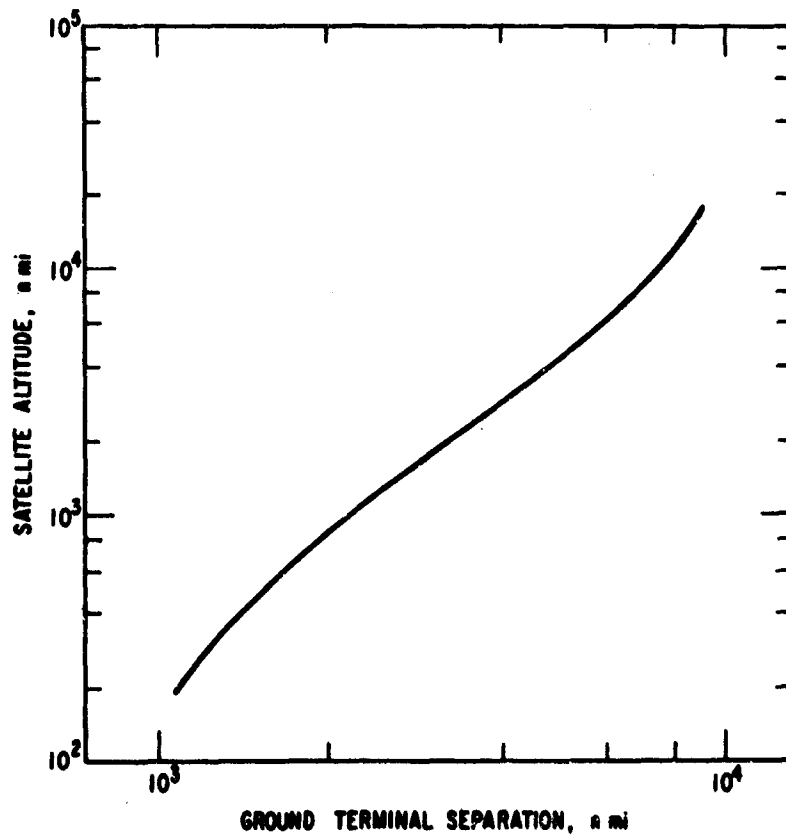


**Fig. 45. Ground Terminal Separation vs
Satellite Altitude for Mutual Visibility**

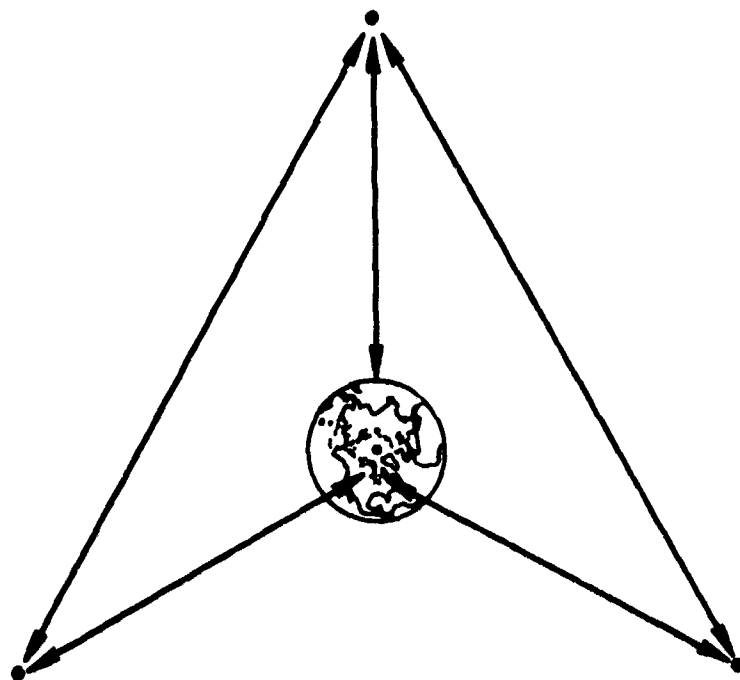


Fig. 46. Global Coverage Relay System

C. MILLIMETER-WAVE COMMUNICATION

The discussion, thus far, has dealt with orbital factors. Since this paper is concerned with millimeter-wave system applications, it is appropriate to ask the following question: What are the advantages of using millimeter waves for this type of communication system? The specific advantage of millimeter waves is the large data bandwidth that it is theoretically feasible.

In any communication system, the data bandwidth is a function of antenna size and frequency if all other factors are equal. However, all factors that affect system performance vary with frequency, and further consideration must therefore be given to these factors. Included are receiver noise figure, power sources, feasible antenna gains, and antenna pointing.

In the space relay system previously indicated (Figure 46), the satellite-to-satellite and the satellite-to-ground terminal links must be examined separately, since atmospheric properties significantly influence the latter, particularly oxygen and water-vapor absorption.

1. SATELLITE-TO-GROUND LINK

In the satellite-to-ground link, environmental factors (for all weather operation) favor the lower frequencies, e.g., 8 GHz as opposed to 35 GHz. Heavy rain causes severe attenuation above 8 GHz, but location diversity of ground terminals can reduce this problem since heavy rains tend to be localized. Water vapor and light rain become a serious problem at frequencies above 35 GHz. For the satellite-to-ground link, therefore, it will suffice to consider two frequencies in order to determine the data bandwidth of presently feasible systems, namely, 8-GHz and the 35-GHz window.

In any satellite-to-ground link, the "down" link will be bandwidth-limited before the "up" link because power available for the satellite transmitter will be much less than that available for the ground terminal transmitter. The maximum size of the satellite antenna is determined by such factors as booster vehicle shroud dimensions and the number of satellites per launch. It should be noted that "foldout" antenna configurations can be employed to increase antenna effective area on deployment. The significant factor concerning satellite antennas is not so much a matter of size, but gain; i.e., a large antenna at lower frequency can have gain comparable to a much smaller antenna at higher frequency, since the surface tolerance allowable is a function of frequency.

In the case of the satellite-to-ground link, what are realistic values of satellite antenna size and transmitter power at the two frequencies under consideration (8 GHz and 35 GHz) with the existing technology status?

A 10-ft partial foldout parabola for 8 GHz and a 5-ft parabola for 35 GHz are considered feasible. Transmitter power of 20 W is achievable in space-qualified TWTAs at both frequencies, although the 35-GHz tube is farther away in time as an available item. The efficiencies of these tubes would not differ significantly.

The ground terminal antenna size is dictated more in terms of economics rather than technology; therefore, in order to evaluate the performance of the postulated link, a 30-ft parabola can be assumed.

Figure 47 summarizes the communication-link performance employing the foregoing assumptions and ground terminal locations compatible with Figure 46. Weather margins for the two frequencies are included, assuming

| | <u>8 GHz</u> | <u>35 GHz</u> |
|--|--------------|---------------|
| SATELLITE TRANSMITTER POWER (20 W) | +43 dBm | +43 dBm |
| SATELLITE ANTENNA GAIN (10-ft PARABOLA) | +45 dB | |
| (5-ft PARABOLA) | | +53 dB |
| GROUND TERMINAL ANTENNA GAIN (30-ft PARABOLA) | +55 dB | +67 dB |
| PATH LOSS ($\approx 22,000$ nmi) | -203 dB | -215 dB |
| MISCELLANEOUS RF LOSSES (WAVEGUIDE, DIPLEXERS, ETC.) | -3 dB | -3 dB |
| POWER AT RECEIVER INPUT PORT | -63 dBm | -55 dBm |
| (NOISE POWER)/Hz (KT) | -174 dBm/Hz | -174 dBm/Hz |
| RECEIVING SYSTEM NOISE FIGURE (PARAMETRIC AMPLIFIER) | 5 dB | 8 dB |
| (PREDETECTION NOISE POWER)/Hz | -169 dBm/Hz | -166 dBm/Hz |
| SIGNAL-TO-NOISE POWER RATIO IN 1-Hz BANDWIDTH | +106 dB | +111 dB |
| REQUIRED SIGNAL-TO-NOISE POWER DENSITY | 13 dB | 13 dB |
| (FOR BIT ERROR PROBABILITY $< 10^{-6}$) | | |
| SYSTEM MARGIN | 3 dB | 3 dB |
| WEATHER MARGIN | 1 dB | 8 dB |
| AVAILABLE BANDWIDTH | 89 dB | 87 dB |
| | 800 MHz | 500 MHz |

**Fig. 47. Communication Link Performance Summary
Satellite-to-Ground Terminal**

moderate antenna look angles and light rain (\sim 5-km path through rain) [2].

The margins given are only for the rain path assumed; considerably more margin would be required for the 35-GHz link under conditions of heavy rain and low antenna look angle. Since the data baseband is equal to one-half of the predetection bandwidth, it follows for digital data and low index angle modulation that the bit rate (megabits/sec) is equal to the predetection bandwidth (MHz). Consequently, for low index-angle modulation a data rate of 800 megabits/s can be accommodated over the 8-GHz link and 500 megabits/s can be accommodated over the 35-GHz link. (Figure 47).

2. SATELLITE-TO-SATELLITE LINK

The satellite-to-satellite link in free space is not affected by the environmental factors that are significant in the satellite-to-ground terminal link. In theory, all other factors being equal, and for a fixed antenna aperture on each satellite, the data bandwidth increases with frequency. Unfortunately, practical technological factors impose limits.

As the carrier frequency is increased, the tolerance on antenna surfaces becomes more severe. This problem is complicated by the nonuniform thermal heating of antenna surface and structures in the space environment. The smaller the antenna beamwidth (for a fixed antenna aperture the beamwidth decreases and the gain increases with increasing frequency), the more difficult is the pointing problem. Receiver noise performance varies inversely with frequency, although not at a rapid rate. The power available from RF sources previously discussed also becomes limited as frequency increases. With the interplay of these many parameters, how does data bandwidth relate to frequency?

The answer to this question must reflect the state of the technology. Presently, the data bandwidth can be considered to increase with frequency to the region where device and component performance becomes the limiting parameter. A curve could be hypothesized to show this type of relationship, but its value would at most be questionable. With a goal of maximum bandwidth, what then is a sensible approach in selecting an operating frequency and the subsequent formulation of a system? The answer perhaps lies in recognizing the technology status that presently exists, as well as near-term forecasts of improvements in the various frequency bands, and then selecting frequencies wherein the technology permits feasible system formulation.

Considerable effort has been devoted to device, component, and subsystem development to 35 GHz. To a lesser degree, development efforts have been extended to 94 GHz. Applied research has been conducted beyond 220 GHz. Therefore, the choice of frequency must necessarily revert to development time and subsequent cost. If "shielding" from earth is desired, the oxygen absorption characteristics of the 60-GHz region can be employed. If the ultimate in data bandwidth in the next five years is set as a goal, with cost as a lesser criterion and the shielding effect of 60 GHz is not a requisite, then, engineering judgment would indicate the 70-GHz region as the highest frequency and a promising choice based on the present state of the technology.

Having thus selected 70 GHz as an operating frequency, what data bandwidths can be accommodated in a feasible system? Figure 48 summarizes the system performance with consideration of the following: A 5-ft antenna for 70 GHz is about the maximum size in which surface tolerances can be maintained

| | |
|--|--------------|
| SATELLITE TRANSMITTER POWER (20 W) | +43 dBm |
| SATELLITE TRANSMITTING ANTENNA GAIN (5-ft PARABOLA) | +58 dB |
| RECEIVING ANTENNA GAIN (5-ft PARABOLA) | +58 dB |
| PATH LOSS ($\approx 39,500$ nmi) | -227 dB |
| MISCELLANEOUS RF LOSSES (WAVEGUIDE, DIPLEXERS, ETC.) | -3 dB |
| POWER AT RECEIVER INPUT PORT | -71 dBm |
| (NOISE POWER)/Hz (KT) | -174 dBm/Hz |
| RECEIVING SYSTEM NOISE FIGURE | 10 dB |
| (PREDETECTION NOISE POWER)/Hz | -164 dBm/Hz |
| SIGNAL-TO-NOISE POWER RATIO IN 1-Hz BANDWIDTH | +93 dB |
| REQUIRED SIGNAL-TO-NOISE POWER DENSITY (FOR BIT ERROR PROBABILITY $< 10^{-5}$) | 13 dB |
| SYSTEM MARGIN | 3 dB |
| AVAILABLE BANDWIDTH* | 77 dB 50 MHz |

*THIS BANDWIDTH WILL PERMIT A DATA RATE OF 50 megabits/s
FOR LOW INDEX ANGLE MODULATION

**Fig. 48. Communication Link Performance Summary
Satellite-to-Satellite Relay (70 GHz)**

satisfactorily in space and for which pointing is compatible with the state of the art in attitude-control and steering technology. A 10-dB system noise figure and a 20-W transmitter (TWTA) are also considered near-term achievable device goals. This figure shows that, for low index-angle modulation, a data rate of 50 megabits/s can be accommodated over this link. Comparing the satellite-to-satellite link performance summarized in Figure 48 with the satellite-to-ground link summarized in Figure 47, it is evident that the satellite-to-satellite link, as might be expected, limits the overall system performance. However, the greater bandwidth capability of the satellite-to-ground link permits the simultaneous use of this link by several satellites.

VI. CONCLUSIONS

In the past two to three years, great strides have been made in the development of millimeter-wave technology. The increasing availability of precision antennas, waveguide components, low-noise devices, solid-state sources, and high-power tubes are striking evidence of growing interest and development activity. Moreover, many of the new components are more reliable and are available at greatly reduced cost, which forecasts greater systems applicability.

Recent advances in the development of sensitive millimeter-wave detectors are particularly noteworthy. For example, parametric amplifiers have been constructed and have been demonstrated at 70 GHz and at even higher frequencies; a result of new developments in varactors, diodes, and solid-state sources. Work at the Bell Telephone Laboratories has produced 8-dB noise figures in the 60-GHz region and 9-dB system noise figures at 94 GHz with Schottky barrier diodes. Low-noise point-contact mixer diodes have been developed at The Aerospace Corporation for use at 94 GHz that have overcome a major problem of these devices in the past, i.e., a very short useful lifetime, sometimes less than a week. The Aerospace Corporation diodes utilize gold alloy whiskers on heavily doped GaAs semiconductor material and have exhibited system noise figures near 10 dB, with lifetimes exceeding 10,000 h.

The millimeter-wave region is being viewed with renewed interest by systems people planning new programs. The future for millimeter waves appears very promising.

APPENDIX A

A linearity requirement estimate for repeatable FM sweeps of a large time-bandwidth radar correlator is made as follows. Let the reference pulse be defined as

$$e_r(t) = p(t) \cos \left\{ 2\pi \left[f_0 t + \left(\frac{k}{2} \right) t^2 + \int_0^t f(t') dt' \right] + \theta \right\} \quad (1)$$

where $p(t)$ = envelope or pulsing function (ideal)

f_0 = unmodulated carrier frequency, cps

k = frequency slope of the FM waveform, cps/s²

$f(t')$ = deviation from linear frequency sweep, cps

θ = phase constant, rad

The mixing product for this reference pulse and a normalized target return pulse displaced by τ seconds is (eliminating the sum frequencies)

$$e_m(t) = \frac{p(t) p(t - \tau)}{2} \cos \left[2\pi \left(f_0 \tau + k\tau t - \frac{k\tau^2}{2} \right) + 2\pi \int_0^t f(t') dt' - 2\pi \int_0^{t-\tau} f(t') dt' \right] \quad (2)$$

The expression $2\pi f_0 \tau - 2\pi k\tau^2/2$ represents a phase constant that will be denoted as θ_0 . The expression $2\pi k\tau t$ is representative of the desired constant beat frequency $k\tau$ and will be expressed as wt , where $w = 2\pi k\tau$. The integral expressions, representing the undesired phase deviation (noise spectrum), may be combined as

$$\phi(t) = 2\pi \int_{t-\tau}^t f(t') dt' \quad (3)$$

Thus we have, finally,

$$e_m(t) = g(t, \tau) \cos [wt + \theta_0 + \phi(t)] \quad (4)$$

where

$$g(t, \tau) = [p(t) p(t - \tau)]/2$$

Expanding (4), we obtain

$$e_m(t) = g(t, \tau) [\cos \phi(t) \cos (wt + \theta_0) - \sin \phi(t) \sin (wt + \theta_0)] \quad (5)$$

and from (4) it is seen that $\phi(t)$ must be small to maintain the main response to noise sideband power ratio at a reasonable value. Then, (5) may be written

$$e_m(t) = g(t, \tau) \{ [1 - \phi^2(t)/2] \cos(wt + \theta_0) - \phi(t) \sin(wt + \theta_0) \} \quad (6)$$

The matched filter response is, to the first approximation, proportional to $1 - \phi^2(t)/2$, since the sine term results in a broadband low-level spectrum compared to the narrow-band main lobe response. Thus, the peak of the filter response is down to $1 - \phi^2(t)/2$ from unity.

The power in the main lobe response relative to unity is then given approximately by

$$(1 - \overline{\phi^2}/2)^2 \approx 1 - \overline{\phi^2} \quad (7)$$

where $\overline{\phi^2}$ is the rms value of $\phi^2(t)$. The power in the sidelobes is approximately $\overline{\phi^2}$ on the same relative scale. The exact distribution of sidelobe energy

APPENDIX A

A linearity requirement estimate for repeatable FM sweeps of a large time-bandwidth radar correlator is made as follows. Let the reference pulse be defined as

$$e_r(t) = p(t) \cos \left\{ 2\pi \left[f_0 t + \left(\frac{k}{2} \right) t^2 + \int_0^t f(t') dt' \right] + \theta \right\} \quad (1)$$

where $p(t)$ = envelope or pulsing function (ideal)

f_0 = unmodulated carrier frequency, cps

k = frequency slope of the FM waveform, cps/s²

$f(t')$ = deviation from linear frequency sweep, cps

θ = phase constant, rad

The mixing product for this reference pulse and a normalized target return pulse displaced by τ seconds is (eliminating the sum frequencies)

$$e_m(t) = \frac{p(t) p(t - \tau)}{2} \cos \left[2\pi \left(f_0 \tau + k\tau t - \frac{k\tau^2}{2} \right) + 2\pi \int_0^t f(t') dt' - 2\pi \int_0^{t-\tau} f(t') dt' \right] \quad (2)$$

The expression $2\pi f_0 \tau - 2\pi k\tau^2/2$ represents a phase constant that will be denoted as θ_0 . The expression $2\pi k\tau t$ is representative of the desired constant beat frequency $k\tau$ and will be expressed as wt , where $w = 2\pi k\tau$. The integral expressions, representing the undesired phase deviation (noise spectrum), may be combined as

$$\phi(t) = 2\pi \int_{t-\tau}^t f(t') dt' \quad (3)$$

Thus we have, finally,

$$e_m(t) = g(t, \tau) \cos [wt + \theta_0 + \phi(t)] \quad (4)$$

where

$$g(t, \tau) = [p(t) p(t - \tau)]/2$$

Expanding (4), we obtain

$$e_m(t) = g(t, \tau) [\cos \phi(t) \cos (wt + \theta_0) - \sin \phi(t) \sin (wt + \theta_0)] \quad (5)$$

and from (4) it is seen that $\phi(t)$ must be small to maintain the main response to noise sideband power ratio at a reasonable value. Then, (5) may be written

$$e_m(t) = g(t, \tau) \{ [1 - \phi^2(t)/2] \cos(wt + \theta_0) - \phi(t) \sin(wt + \theta_0) \} \quad (6)$$

The matched filter response is, to the first approximation, proportional to $1 - \phi^2(t)/2$, since the sine term results in a broadband low-level spectrum compared to the narrow-band main lobe response. Thus, the peak of the filter response is down to $1 - \phi^2(t)/2$ from unity.

The power in the main lobe response relative to unity is then given approximately by

$$(1 - \overline{\phi^2}/2)^2 \approx 1 - \overline{\phi^2} \quad (7)$$

where $\overline{\phi^2}$ is the rms value of $\phi^2(t)$. The power in the sidelobes is approximately $\overline{\phi^2}$ on the same relative scale. The exact distribution of sidelobe energy

depends on $\phi(t)$. However, a crude but reasonable criterion is that the total sidelobe power be down from the main lobe power by ~ 20 dB. Then

$$\phi^2 \leq 0.01$$

and

$$\bar{\phi} \leq 0.1 \approx 6 \text{ deg rms}$$

From (3), one may now obtain an estimate on the rms frequency deviation that is tolerable, upon making the assumption of essentially constant $f(t')$ over the short integration interval of $(t - \tau \text{ to } t) = \tau$ seconds. Then, from (3) one finds

$$\begin{aligned} \phi(t) &= 2\pi t' f(t') \Big|_{t-\tau}^t \\ &= 2\pi \tau f(t) \end{aligned}$$

Taking $\tau = 10^{-7}$ s, corresponding to a range window of ± 50 ft, one finds

$$f_{\text{rms}} = \frac{0.1}{2\pi \times 10^{-7}} \approx 160 \text{ kHz}$$

The phase-locked system employed for linearization must maintain a loop error to within 6 deg rms over the sweep interval to meet the stated criterion.

APPENDIX B

The bandwidth of the phase-lock loop must be maintained at a value less than the frequency at which the phase shift around the loop is 90 deg. Otherwise, the loop will oscillate at the frequency at which the phase shift becomes 90 deg. The total phase shift is composed of amplifier and filter phase shifts and phase components due to propagation delay τ_p and phase detector delay τ_ϕ . If it is assumed that amplifier and filter phase shifts are small compared to the phase shifts due to time delay, then it becomes desirable to optimise the system for minimum time delay. Let the loop time delay be defined as

$$\tau = \tau_p + \tau_\phi$$

where τ = total time delay around the loop, s

τ_p = range propagation delay, s

τ_ϕ = phase detector delay, s

For the proposed radar, an FM sweep rate of 1000 MHz/ms has been selected. This is equivalent to 10^{12} Hz/s. Thus, the beat frequency f_b from the linearising homodyne receiver can be expressed as

$$f_b = 10^{12} \tau_p$$

A sample and hold phase detector has been developed for use in the loop because of its inherent broad bandwidth characteristics. The signal delay τ_ϕ of the phase detector is one-half the storage time. This is expressed as

$$\tau_{\phi} = 1/2nf_b$$

where n is the number of samples per cycle of the reference frequency.

Expressed in terms of propagation delay, this is

$$\tau_{\phi} = 10^{-12}/2n\tau_p$$

and

$$\tau = \tau_p + \left(10^{-12}/2n\tau_p\right)$$

Differentiating to determine the conditions for minimum τ , one finds

$$d\tau/d\tau_p = 1 - 10^{-12}/2n\tau_p^2 = 0$$

$$\tau_p^2 = 10^{-12}/2n$$

$$\tau_p = \tau_{\phi} = 1/\sqrt{2n} \times 10^{-6} \text{ s}$$

As expected, the minimum occurs when the two delays are equal. By the use of a phase detector that takes two samples per cycle ($n = 2$), the optimum propagation and phase detector delays are

$$\tau_d = \tau_{\phi} = 1/\sqrt{4} \times 10^{-6} = 0.5 \mu\text{s}$$

The maximum loop bandwidth is the frequency at which the total time delay results in 90-deg phase shift

$$f_{\max} = 1/4\tau = 250 \text{ kHz}$$

Similarly, if a four-sample-per-cycle phase detector is employed, the optimum parameters are

$$\tau_d = \tau_\phi = 10^{-6} / \sqrt{8} = 0.353 \mu s$$

$$\tau = 0.706 \mu s$$

$$f_{\max} = 353 \text{ kHz}$$

REFERENCES

- [1] H. C. van de Hulst, Light Scattering by Small Particles. New York: Wiley, 1957.
- [2] R. L. Mitchell, "Radar meteorology at millimeter wavelengths," Aerospace Corporation, TR-669(6230-46)-9, June 1966.
- [3] C. R. Burrows and S. S. Atwood, Radio Wave Propagation. New York: Academic Press, 1949, p. 48.
- [4] G. E. Weibel and H. O. Dressel, "Propagation Studies in Millimeter Wave Links," Proc. IEEE, vol. 55, No. 4, April 1967.
- [5] E. S. Rosenblum, "Atmospheric absorption of 10-400 kMcps radiation," Microwave Journal, pp. 91-96, March 1961.
- [6] J. A. Saxon, Advances in Radio Research. New York: Academic Press, 1964, Vol. 1, p. 153.
- [7] E. Altshuler, Earth-to-space communications at millimeter wavelengths, Air Force Cambridge Research Laboratories, Bedford, Mass, (to be published).
- [8] F. K. Smith and S. Weintraub, "The constant in the equation for atmospheric refractive index at radio frequencies," Proc. IRE, vol. 41, pp. 1035-1037, August 1953.
- [9] R. L. Mitchell, "Antenna radiation characteristics with partially coherent radiation," IEEE Trans. on Antennas and Propagation, vol. AP-14, pp. 324-329, May 1966.

- [10] H. E. King, E. Jacobs, and J. M. Stacey, "A 2.8 arc-min. beamwidth antenna; lunar eclipse observations at 3.2 mm," IEEE Trans. on Antennas and Propagation, vol. AP-14, pp. 82-91, January 1966.
- [11] G. R. Heildreder, "Image degradation with random wavefront tilt compensation," IEEE Trans. on Antennas and Propagation, vol. AP-15, pp. 90-98, January 1967.
- [12] R. D. Etcheverry, G. R. Heildreder, W. A. Johnson, and H. J. Wintroub, "Measurements of spatial coherence in 3.2-mm horizontal transmission," IEEE Trans. on Antennas and Propagation, vol. AP-15, pp. 136-141, January 1967.
- [13] L. A. Hoffman, H. J. Wintroub, and W. A. Garber, "Propagation observations at 3.2 millimeters," Proc. IEEE, vol. 54, pp. 449-454, April 1966.
- [14] L. A. Hoffman, "Propagation factors at 3.2 millimeters," 10th AGARD/NATO Symposium on Propagation Factors in Space Communications, Rome, Italy, September 1965; also, Aerospace Corporation, TDR-469(5230-41)-6, October 1965.
- [15] A. W. Rihaczek and R. L. Mitchell, "A high-resolution approach to satellite identification," Ground Identification of Satellites (GISAT) Symposium, Bedford, Mass., 2-4 October, 1967.

UNCLASSIFIED
Security Classification

| DOCUMENT CONTROL DATA - R&D | | |
|---|--|--|
| <i>(Security classification of title, body of abstract and indexing annotation must be entered when the overall report is classified)</i> | | |
| 1. ORIGINATING ACTIVITY (Corporate author) Aerospace Corporation El Segundo, California | | 2a. REPORT SECURITY CLASSIFICATION Unclassified |
| | | 2b. GROUP |
| 3. REPORT TITLE MILLIMETER-WAVE PROPAGATION AND SYSTEMS CONSIDERATIONS | | |
| 4. DESCRIPTIVE NOTES (Type of report and inclusive dates) | | |
| 5. AUTHOR(S) (Last name, first name, initial) Hoffman, L. A. | | |
| 6. REPORT DATE October 1968 | 7a. TOTAL NO. OF PAGES 94 | 7b. NO. OF REFS 15 |
| 8a. CONTRACT OR GRANT NO. F04701-68-C-0200 | 9a. ORIGINATOR'S REPORT NUMBER(S) TR-0200(4230-46)-1 | |
| b. PROJECT NO. | | |
| c. | 9b. OTHER REPORT NO(S) (Any other numbers that may be assigned this report) SAMSO-TR-68-445 | |
| d. | | |
| 10. AVAILABILITY/LIMITATION NOTICES This document has been approved for public release and sale; its distribution is unlimited. | | |
| 11. SUPPLEMENTARY NOTES | 12. SPONSORING MILITARY ACTIVITY Space and Missile Systems Organization Air Force Systems Command Los Angeles, California | |
| 13. ABSTRACT Applications for millimeter waves are discussed, and it is shown how propagation effects enter into systems considerations for the EHF region. The state of the millimeter-wave art is reviewed as to antennas, sources, amplifiers, and receivers. Highlighted are two applications, a high-resolution radar, which it is hoped can utilize the inherent advantage of the short millimeter wavelengths for resolution, and a space-to-space communication system at EHF. | | |

DD FORM 1472
(FACSIMILE)

UNCLASSIFIED
Security Classification

14.

KEY WORDS

Communication
EHF Applications
Millimeter Waves
Propagation Effects
Radar

Abstract (Continued)